Journal of Molecular Structure 1078 (2014) 26–42

Contents lists available at ScienceDirect

Journal of Molecular Structure

journal homepage: www.elsevier.com/locate/molstruc

A molecular picture of the problems in ensuring structural purity of tazofelone

Louise S. Price [a], Jennifer A. McMahon [b], Sreenivas R. Lingireddy [b], Suk-Fai Lau [b], Benjamin A. Diseroad [b], Sarah L. Price [a], Susan M. Reutzel-Edens [b,*]

[a] Department of Chemistry, University College London, 20 Gordon Street, London WC1H 0AJ, UK
[b] Lilly Research Laboratories, Eli Lilly and Company, Lilly Corporate Centre, Indianapolis, IN 46285, USA

HIGHLIGHTS

- The computed crystal energy landscape suggests problems with structural purity.
- Attempts to obtain phase pure form RCI found closely related RCIII.
- Difficulties in obtaining structural purity extends to single crystals.
- Racemic solid solution seeded by enantiopure form rationalized.
- Modern techniques show variability in thermal properties, etc. can be unavoidable.

GRAPHICAL ABSTRACT

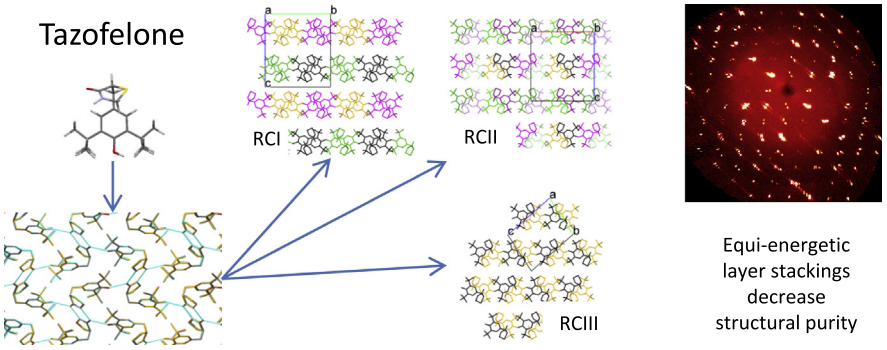

ARTICLE INFO

Article history:
Available online 18 January 2014

Keywords:
Tazofelone
Solid form screening
Crystal structure prediction
Disorder
Polymorphism
Structural purity

ABSTRACT

Almost twenty years after the crystal polymorphism of tazofelone was first studied at Lilly, the compound was revisited by calculating the crystal energy landscape and complementing the calculations with experimental work for calibration purposes. The crystal structure prediction study confirmed the stability of racemic form II (RCII) and showed that the racemic compound had greater potential for polymorphism than the single enantiomer. The seeding experiment that has previously been shown to produce a racemic solid solution (SS) correlates with the isostructurality between some low energy racemic structures and the enantiopure form. Other low energy structures have the same layer structure as both racemic polymorphs and the newly-discovered, but closely related, polymorph RCIII, which accounts for the difficulty in obtaining phase pure samples of the metastable RCI and RCIII and the problems of structural purity evidenced by streaked diffraction spots for RCI–III in the single crystal diffraction. This molecular picture of the problems in ensuring structural purity in the layer structure polymorphs of tazofelone not only explains the crystal dependent thermochemistry measurements of tazofelone, but also shows the value of combining a range of experimental and computational techniques to investigate the organic solid state.

1. Introduction

Solid form screening in the pharmaceutical industry seeks to identify all practically important solid forms of a molecule, particularly the most stable, determine their structures and properties and define conditions for obtaining phase-pure samples. The experimental form landscapes that emerge from industrial solid form screens inevitably rely on surveying diverse crystallization conditions and carefully applying many different solid-state characterization techniques to unequivocally distinguish bonafide crystal forms from sample dependent variability. Crystallization processes are then developed to select for the preferred form,

* Corresponding author. Address: Small Molecule Design & Development, Lilly Research Laboratories, Eli Lilly and Company, Lilly Corporate Centre, Indianapolis, IN 46285, USA. Tel.: +1 (317) 276 0994; fax: +1 (317) 277 8387.
E-mail address: reutzel-edens_susan_m@lilly.com (S.M. Reutzel-Edens).

0022-2860/$ - see front matter © 2014 Elsevier B.V. All rights reserved.
http://dx.doi.org/10.1016/j.molstruc.2014.01.014

producing bulk materials that perfectly match, usually by powder X-ray diffraction, the crystal form reference. The ensuing development of the solid form is usually based on the assumption that consistency in powder X-ray diffraction means that microcrystalline samples have the same structure as the single crystals, and all samples approximate the ideal of structural purity, i.e. exhibit the same 3D molecular arrangement in every particle [1]. Recent examples, such as aspirin Form II [2], have highlighted, however, the sometimes fine line that differentiates a very similar polymorph from a defective or modulated structure. Such systems require in-depth understanding of the origins of defects and disorder at a molecular level that is both a challenge to existing methodologies and an opportunity for developing new approaches.

Crystal Structure Prediction (CSP) methods for generating the low energy crystal structures of a molecule from its chemical diagram were first developed to confirm whether the most stable crystal structure was known [3,4]. The crystal energy landscape, the set of structures which are sufficiently low in energy to be thermodynamically plausible as polymorphs, has been shown to be useful [5] for suggesting experiments to find more polymorphs, helping to characterize new forms or suggest the potential existence of disordered phases [6], and generally complementing solid form screening. The last blind test of CSP [7] lead to the rapid development of methods for evaluating the crystal energy landscape for larger flexible molecules, by having benzyl-(4-(4-methyl-5-(p-tolylsulfonyl)-1,3-thiazol-2-yl)phenyl)carbamate as a target, whose structure was successfully predicted [8]. Since then, CSP methods have been applied and tested by contrasting the crystal energy landscapes of a few pharmaceutical molecules with industrial screening results [9–11]. The current study was undertaken to continue this assessment of the practical utility of crystal energy landscapes as a component of industrial-style solid form screening by application to tazofelone (Fig. 1). Tazofelone (TZF, 2,6-di-tert-butyl-4-(1,3-thiazolidin-5-ylmethyl)phenol) is a potent antioxidant and 5-lipoxygenase inhibitor which was originally investigated at Lilly two decades ago as a novel therapy for inflammatory bowel diseases [12].

Tazofelone (TZF) was chosen for study because of its established [13,14] unusual crystallization behaviour. A racemic liquid of TZF was believed to crystallize spontaneously as one of two enantiotropically related racemates. However, if seeds of the only known enantiopure form are introduced to a melt, a type II solid solution with a structure resembling that of the enantiomorph is formed. This solid solution is important as it provides a higher solubility alternative to the racemate (though lower solubility than the enantiomorph) for formulating and delivering TZF. However, its discovery by seeding is a variation of cross-nucleation between polymorphs [15–17], illustrating how seeding can be used to discover and engineer crystal forms. Would the crystal energy landscape for TZF have suggested that such a seeding experiment was worth trying in the search for novel solid forms? Does it indicate that other potential polymorphs might be found, particularly since enantiopure TZF has not been subjected to a polymorph screen?

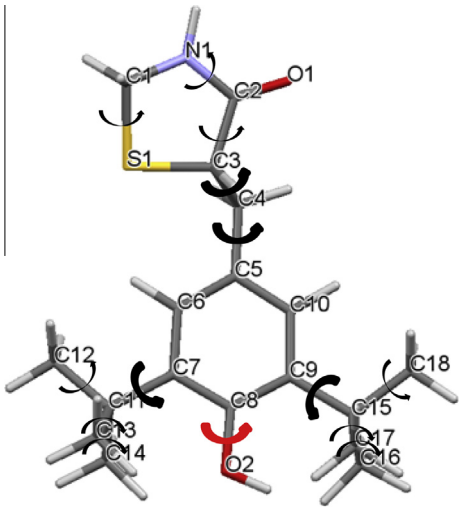

Fig. 1. S-Tazofelone (TZF) (LY231696) with the atomic numbering used in this work. C3 is the chiral centre, defining S. The R enantiomer is LY231697 and the racemic compound is LY213829. The 5 torsion angles which were varied in the CrystalPredictor search for potential structures are marked in bold, and the other angles which were refined in the last stages (by CrystalOptimizer) in weaker arrows. The red arrow denotes the torsion angle whose variation between structures was particularly accurately modelled, by using gradients of the multipole moments, in the CrystalOptimizer refinement.

This study is building on detailed investigations of the structures and thermodynamic relationships of the solid forms of TZF, carried out 15–20 years ago [13,14]. Those investigations characterized the structures of two racemic polymorphs (denoted RCII and RCI), an enantiopure structure (AS), and the racemic solid solution, and provided some thermodynamic data. The racemic forms RCI ($P2_1/c$) and RCII (*Pbca*) are based on hydrogen bonded layers of the molecules in the folded conformation. The melting points, heats of fusion and eutectic melting data indicated that the racemic forms are enantiotropically-related, with RCII being more stable at low temperatures. Mixtures of RCI and RCII are obtained at crystallization temperatures significantly below the transition temperature which even at that time varied but was given as 138 °C, indicating that the crystallization of racemic TZF is kinetically-driven. The enthalpy difference between RCI and RCII was estimated as 2.7 kJ mol^{-1} and the free energy difference is relatively small even well below the transition temperature. The resultant difficulty in avoiding supersaturating solutions with respect to both polymorphs in crystallization and hence tendency for concomitant crystallization means that racemic TZF is a system where structural insights should be important in determining the processing, properties and performance of the drug product [18,19]. This study revisited the racemic system, initially expecting just to extend the enthalpy estimates and error assessment to lower temperatures through heat capacity measurements as a means of calibrating the computational work. However, modern techniques of physical characterization revealed that providing phase-pure samples and sample-consistent thermodynamic data to modern standards was not possible. Hence, this study illustrates the issue of "structural purity" [1] in drug development.

The solid solution (SS-0.5, WIMBAV07, Table 1) is isostructural with the enantiomorph crystal structure (AS, WILZUM) which templates its crystallization. The $Z' = 2$ enantiomorph crystal structure has the molecule in two different conformations, A and B (as defined in [13,14]), while the $Z' = 1$ solid solution has the molecule in one of these conformations at each site. The inversion symmetry of the space group relates the molecules, but the lower temperature determination deviates from a 50:50 disorder. The remarkable spatial similarity of a conformation A molecule with R chirality and a conformation B molecule with S chirality (Fig. 2a) demonstrates how perfectly molecules of the opposite "hand" can be incorporated into the structure of the enantiopure crystal. This leads to a continuum of solid solutions [20] between the conglomerate and the 50:50 mixture, of which the latter could be termed a racemic polymorph, as it gives the same melt as RCI and RCII, at only a slightly lower temperature. For clarity, this polymorph SS-0.5 will be referred to as SSIV. The most stable racemate, RCII, and the conglomerate of the two equivalent enantiopure crystals, AS and AR, are monotropically related, with the higher melting RCII being more stable at any temperature. The energy difference between RCII and the conglomerate has been measured by eutectic melting

Table 1
Summary of crystallographic results with previous published work on TZF crystals [13,14], defining notation and derived structures.

Crystal structure CSD refcode and notation	Space group Z' (Z)	Temp. (K)	a (Å)	b (Å)	c (Å)	α (°)	β (°)	γ (°)	Density (Mg m^{-3})
Racemate II RCII low temperature polymorph	*Pbca* 1 (8)	100	17.1102(3)	11.0958(2)	18.6504(4)	90	90	90	1.206
		296	17.1967(4)	11.2756(3)	18.8057(5)	90	90	90	1.171
WIMBAV [13]/1a-II		RT	17.204(3)	11.287(3)	18.860(7)	90	90	90	1.166
Racemate I RCI first high temperature polymorph	$P2_1/c$ 2 (8)	100	11.0992(3)	16.9748(5)	19.2201(5)	90	100.5695(16)	90	1.200
		296	11.3103(6)	17.0578(9)	19.3296(10)	90	101.029(3)	90	1.167
WIMBAV01 [13]/1a-I I		RT	11.313(3)	17.082(4)	19.324(7)	90	101.11(2)	90	1.165
Racemate III RCIII second high temperature polymorph	*P*-1 2 (4)	100	11.1050(4)	11.8502(5)	14.9408(6)	77.672(2)	75.185(2)	71.440(2)	1.197
		296	11.2917(5)	11.9167(6)	14.9597(7)	77.827(3)	75.208(3)	71.585(3)	1.168
Enantiomorph R-Tazofelone AR	$P2_1$ 2 (4)	100	9.1732(2)	10.9437(2)	17.6317(4)	90	93.8103(12)	90	1.209
		296	9.4100(4)	10.9705(4)	17.8316(7)	90	94.315(3)	90	1.163
S-Tazofelone AS WILZUM [13]/1b		RT	9.392(2)	10.962(2)	17.823(4)	90	94.29(3)	90	1.167
Racemic Solid solution WIMBAV07 [14]/SS-0.5/0.57:0.43 S:R disorder	$P2_1/n$ 1 (4)	100	9.2106(7)	10.9363(7)	17.6476(8)	90	93.331(2)	90	1.203
Solid solution WIMBAV06 [14]/SS-0.5 isotropic refinement with 0.50:0.50 S:R disorder Hereafter referred to as polymorph SSIV		296	9.3882(14)	10.9503(16)	17.855(3)	90	93.766(3)	90	1.166

[20] giving an enthalpy difference of 11–12 kJ mol^{-1}. The value of ΔH of the solid solution relative to RCII could only be determined from pure melting data, from which it appears to have a higher free energy than RCI and RCII, but lower free energy than the conglomerate of AR and AS. For computational modelling purposes, the major and minor components of the low temperature solid solution structure WIMBAV07 can be considered as separate ordered Z' = 1 structures SSIV-A and SSIV-B, respectively.

The previous study [13] found that three force-fields were inadequate to represent the crystal structures and relative lattice energies of the three ordered structures AS, RCI and RCII, and that the conformational energies of the molecules, as extracted from the crystal structure, calculated at the RHF/STO-3G and RHF/3-21G* levels varied significantly and were implausibly high for the conformers in the AS structure. There have been significant advances in computational modelling of the organic solid state, with both periodic electronic structure methods and models based on separating the lattice energy into various contributions from the intermolecular forces and conformational energy penalties being under active development through coding more accurate theories. Different methods still give significant differences, sometimes even in the ordering, in the relative stability of polymorphs [21,22], and the accuracy of the approximations in the different approaches are very dependent on the molecule [23,24]. The lattice energy, the energy required to go from the idealized static crystal to infinitely separated static molecules in their lowest energy conformation, is a hypothetical construct, and comparisons with experimental results are based on assumptions about the variations in molecular motions with temperature that are particularly questionable in the case of enantiotropic systems. Hence, as the crystal energy landscape emerged, it seemed worthwhile revisiting TZF experimentally, to measure heat capacities down to −70 °C to provide a better estimate of the lattice energy differences for benchmarking computational methods. Work on preparing fresh samples of racemic TZF polymorphs provided some surprises that required the combination of modern characterization and the hypothetical structures generated by the crystal energy landscape to rationalize.

2. Materials and methods

2.1. Experimental work

Racemic (purity 99.6–99.9%) and enantiopure TZF (R-, purity 92.7%, S-, purity 99.2%) were obtained from Lilly Research Laboratories. Single crystals of RCI, RCII and RCIII were grown, in many instances concomitantly, from toluene by solvent evaporation and cooling. Enantiomer, AR, single crystals were grown by vapour diffusion of heptane into an ethanol solution of R-TZF at ambient temperature. The solid solution, SSIV, was obtained by seeding a supercooled racemic melt with AR (or AS) at 140 °C, following the procedure of Yu et al. [14]. Detailed experimental procedures used to grow TZF single crystals (for the structure determinations) and to recrystallize the most phase pure, highly crystalline bulk samples of the different forms are provided in Supplementary data (Section 1).

Single crystal X-ray diffraction (SXRD) data for TZF RCI, RCII, RCIII and AR were collected at 100 and 296 K for single crystals mounted on thin glass fibers using a Cu Kα radiation source (λ = 1.54178 Å) and a Bruker D8 based 3-circle goniometer diffractometer equipped with a SMART APEX II 6000CCD area detector. Cell refinement and data reduction were accomplished using the SAINT software program [25–27]. Data were corrected for absorption effects using the multi-scan method (SADABS) [28]. The structures were solved by direct methods and refined by full-matrix least squares against F^2 of all data using SHELXTL V6.2 software [27]. Non-hydrogen atoms were refined anisotropically. Hydrogen atoms, which were included in the structure factor calculations, were included as riding in idealized positions (U_{iso}(H) = 1.5 U_{eq}(C) for —CH_3 and U_{iso}(H) = 1.2 U_{eq}(C) for all others) and independently

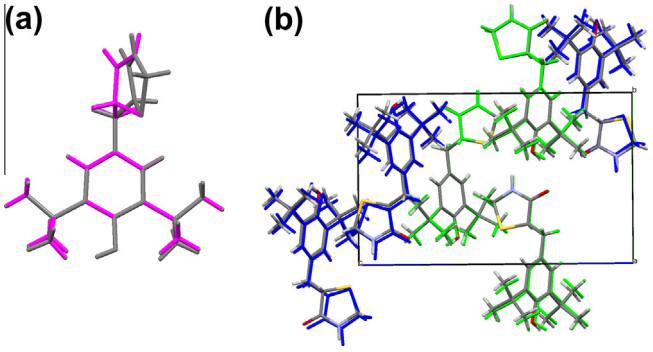

Fig. 2. (a) The solid solution structure WIMBAV07, overlaying the major (0.57) component conformation A (R-configuration, magenta), with the minor (0.43) component conformation B (S-configuration, grey). (b) Overlay of the major component of solid solution structure (WIMBAV07, coloured by element) with the enantiomorph (AR, coloured by symmetry equivalence).

refined. All NH/OH hydrogen atoms, except the NH in RCIII and OH in AR, were located from difference maps and refined isotropically. The absolute stereochemistry of AR was determined by refinement of the absolute structure parameter. PLATON [29] (Unix version, updated on October 25, 2013) showed no additional or missing symmetry in the RCI–III crystal structures. Additional details of the data collection, structure solution and refinement are provided in Table S3.

Powder X-ray diffraction (PXRD) patterns were collected on a Bruker D8 Advance X-ray powder diffractometer, equipped with a monochromatic Cu $K\alpha_1$ source ($\lambda = 1.54056$ Å) and a Linxeye detector, and operating at 40 kV and 40 mA, with a 0.2 mm divergence slit. Each sample was scanned from 4° to 30° in 0.02° 2θ steps at a rate of 0.2 s per step.

Differential scanning calorimetry was conducted using a TA Instruments Q1000 DSC. Samples (~1 to 2 mg) were hermetically-sealed in Tzero aluminum pans, equilibrated at 0 °C, then heated to 190 °C at 10 °C min^{-1} with a 50 mL min^{-1} nitrogen gas purge. The temperature and heat flow were calibrated at 10 °C min^{-1} against indium melting ($T_m = 156.60$ °C, $H_f = 28.57$ J g^{-1}). Melting points were determined to ±0.1 °C (estimated from three successive measurements, Fig. S3 and Table S4) from extrapolated melting endotherm onset temperatures and melting enthalpies to ±0.1 kJ mol^{-1} by peak integration using sigmoidal tangents to define the baseline.

Cross polarization/magic angle spinning (CP/MAS) NMR spectra were obtained on a Bruker Avance III 400 wide-bore NMR spectrometer operating at ^{1}H and ^{13}C frequencies of 400.131 and 100.622 MHz, respectively, and using a Bruker 4 mm triple resonance probe. The MAS rate was set to 10 kHz using a Bruker MAS-II controller; spinning speeds were maintained within 2 Hz of the set point. SPINAL64 [30] decoupling at a proton nutation frequency of 100 kHz was used for heteronuclear decoupling. Spinning sidebands were eliminated by a five-pulse total sideband suppression (TOSS) sequence [31]. The CP contact time for transferring magnetization from protons to carbons was set to 3.0 ms and a RAMP100 shaped H-nucleus CP pulse was used on the ^{1}H channel to enhance CP efficiency [32]. The acquisition time was set to 34 ms and spectra were acquired over a spectral width of 30 kHz with a recycle delay of 3 s. The sample temperature was regulated to 297 ± 1 K in order to minimize frictional heating caused by sample spinning. The ^{13}C chemical shifts were externally referenced (±0.05 ppm) to the proton-decoupled ^{13}C peak of neat (liquid) tetramethylsilane via the high-field resonance of adamantane ($\delta = 29.5$ ppm).

2.2. Isolated molecule energy evaluations and lattice energy calculations

It is a particularly necessary prerequisite for a worthwhile CSP study to confirm that the method of modelling the lattice energy is adequate for the known structures. In this study, the lattice energy, the energy of the static crystal structure relative to infinitely separated molecules in their lowest energy conformation, was calculated from

$$E_{latt} = U_{inter} + \Delta E_{intra},$$

where ΔE_{intra} is the ab initio conformational energy penalty for the change in conformation between the isolated molecule minimum energy and the conformation adopted in the crystal structure, and U_{inter} is the intermolecular lattice energy calculated from an anisotropic atom–atom intermolecular potential. ΔE_{intra} is calculated at the PBE0/6-31G(d,p) level of theory (unless otherwise specified) using GAUSSIAN03 [33]. The same molecular charge density was analyzed using GDMA [34,35] to give a set of atomic distributed multipoles, up to quadrupole, which were used to calculate the electrostatic contribution to the lattice energy, using all terms up to R^{-5} (i.e. including the interaction between the quadrupoles representing the π electron density, etc.). All other terms in the intermolecular lattice energy were calculated from an isotropic exp-6 repulsion–dispersion model, using the FIT parameters [36,37] and *S* parameters for thioethers [38–40]. The program DMACRYS [41] was used to minimize the lattice energy for a given rigid conformation of the molecule. The program CrystalOptimizer [42] was used to minimize E_{latt} as a function of the torsion angles marked on Fig. 1, and the molecular rotations, translations and cell parameters allowed by the space group symmetry, using a database of the ab initio molecular calculations. All lattice energy minima were checked for being genuine minima, by evaluating the Born criterion for mechanical stability.

Investigations of the sensitivity of the calculated lattice energies to the computational model included varying the quality of wavefunction used for ΔE_{intra}, and of calculating the charge distribution in a polarizable continuum model with a dielectric of 3, typical of organic crystals [43].

2.3. Crystal structure prediction

The CrystalPredictor search considered one molecule in the asymmetric unit ($Z' = 1$), 17 enantiopure and 42 racemic space groups and a large conformational region that includes the AB, F and C conformers (Fig. 11) (further details in Supplementary data Section 3). This generated 1 million crystal structures, each of which was minimized using the FIT potential and a set of atomic point charges fitted to the electrostatic potential of the lowest energy conformation, F, at the PBE0/6-31G(d,p) level of theory. All structures within 20 kJ mol^{-1} of the lowest energy structure in each of the three conformational regions (approximately 2500–5000 per region) had ΔE_{intra} re-evaluated and the distributed multipoles calculated at the PBE0/6-31G(d,p) level of theory and were reminimized using DMACRYS. At this stage, the lowest energy structure resembled RCII.

Finally, the lowest 1381 unique structures (within 30 kJ mol^{-1} of the lowest energy structure) were fully optimized using CrystalOptimizer, as described above. Following removal of duplicate structures, 812 structures remained within 30 kJ mol^{-1} of the global minimum.

2.4. Other computational structural comparisons

The comparisons of the structures were done using the tools in Mercury [44], including both analysis by crystallographic symmetry and structural similarity overlays, to determine the largest common cluster ($n \leqslant 15$) that can be overlaid within the default tolerances in interatomic distances and angles, and the corresponding lowest root mean square difference in the non-hydrogen atom–atom distances ($RMSD_n$).

Mercury 3.2.0 Crystal Form Consortium structural or solid form informatics tools were used for analyzing the TZF crystal structures in comparison with the structures in the Cambridge Structural Database (CSD version 5.34 plus November 2012, February 2013 and May 2013 updates). The logit hydrogen bond propensity tool [45] was applied (Supplementary data Section 5.1) to assess the likelihood of pairwise hydrogen bonding interactions based on a statistical analysis of hydrogen bonds in relevant structures in the CSD; Full Interaction Maps (FIMs) were used to explore the degree to which hydrogen bonding interactions were satisfied based on the geometry of the interactions in the racemic and enantiopure crystal structures (Supplementary data Section 5.2) [46]. FIMs are intermolecular interaction density maps generated by superimposing 3D Isostar scatterplots of individual pairs of functional groups onto whole molecules or clusters of molecules, taking into account

steric crowding factors. For TZF, FIMs of hydrogen bond donor and acceptor hotspots were constructed using uncharged NH donor and carbonyl acceptor probes, respectively, to give the probability of finding these interactions above the random chance that they will occur.

3. Results

3.1. Experimental measurements

TZF was initially recrystallized to produce fresh, phase pure samples of RCI, RCII and AR (or AS) for accurate DSC and heat capacity measurements; these data were to be used to assess enthalpy differences between the forms at temperatures as low as experimentally possible within the Lilly laboratory for eventual comparison with computed lattice energy differences. Single crystal growth experiments were also conducted specifically to produce suitable crystals for low temperature X-ray structure determinations, which would facilitate comparisons to 0 K structures on the computed crystal energy landscape. While the crystallization effort was by no means exhaustive (Table S1) and instead focussed on the few solvents that had been used in the early 1990s, a few general trends were noted in the crystallization behaviour of TZF. RCII was selectively recrystallized in polycrystalline form from isopropyl alcohol, ethyl acetate and toluene by slow cooling. The stable form was also obtained in pure form by slurrying mixtures of the RC polymorphs in diverse solvents at moderate temperatures (e.g., 25–60 °C). Metastable RCI, on the other hand, tended to recrystallize from concentrated toluene solutions by rapid cooling and fast solvent evaporation. The experimental conditions which yielded RCI in the most highly crystalline form appeared to be those in which crystallization was slowed, but these conditions often yielded mixtures of the polymorphs, as suggested by the diverse habits of crystals grown well from toluene in 1996 (Fig. 3).

The TZF crystals grown in 1996 were reasonably well preserved over a period of 17 years, but most suffered from the relatively rare problem (at least for pharmaceuticals) of being too large to be used as is for single crystal diffraction. Diffraction data was, however, collected on one crystal from the batch that resembled the smallest individual crystal in Fig. 3 (right, actual crystal shown in Supplementary data Fig. S3) and was suspected to be RCI based on its external shape. Surprisingly, the structure was solved as RCII (crystal data in Supplementary data Section 1.2.1). Attempts were not made to cut the larger 1996 crystals to size, because TZF crystals are highly susceptible to shearing (similar to graphite) with even minimal handling. Instead, smaller single crystals were freshly grown from toluene by slow evaporation. Remarkably, the first crystal retrieved from the new batch for SXRD analysis was shown to be a different form, a third racemic polymorph hereafter referred to as RCIII. The second crystal analyzed from the same batch was RCI. RCII single crystals were also grown from toluene, but in a separate experiment, for SXRD analysis. In the end, single crystals of RCI–III, all crystallized from toluene under very similar conditions, were used to solve the structures of these polymorphic forms of TZF at both 100 and 296 K (Table S3).

RCIII, like RCI and RCII, is comprised of sheets of TZF molecules in similar folded conformations that are connected by $R_2^2(8)$ head-to-head amide–amide interactions and cross-linked by $C_1^1(10)$ hydroxyl–carbonyl interactions (Fig. 4a). The sheets are strikingly similar in each of the RC structures and are only induced to stack in different ways by weak dispersion interactions. The density of RCI–III therefore reflects the close packing of the hydrogen bonded sheets, with the stacking being most efficient and hence the density being the highest for RCII at both 100 and 296 K. RCI is the next most efficiently packed polymorph followed by RCIII at 100 K, but is the least dense at 296 K. Thermal expansion of the crystals is very anisotropic with the greatest changes observed in the cell dimensions defining the layers (Table 1), consistent with the layers being internally "soft".

The crystallographic symmetry relationships of the layer stacking in the observed polymorphs are shown in Fig. 5. If we consider the layer in the mother phase RCII as a two-dimensional periodic fragment (PF) within the Derived Crystal Packing model, then RCI and RCIII can be regarded as daughter phases, where different symmetries contained in the PF have disappeared, giving $Z' = 2$ daughters [47]. The loss in symmetry within the layers in RCI and RCIII is quite slight, with the inversion centre in the RCII sheet becoming an approximate symmetry in the $Z' = 2$ RCI sheet, and the screw axis within the RCII sheet becoming an approximate relationship in the $Z' = 2$ RCIII structure. Adjacent layers in RCII are related by a screw axis. In the daughter phase RCI, the layers are related by an inversion, and in RCIII the relationship is also an inversion, but with the inversion centres between alternate pairs of layers in a different place relative to the molecule (Fig. 4b). Thus the relationship between the PF in RCI and RCIII is quite similar, mainly involving translations of the layers, but the PF is stacked in a distinct manner in RCII.

Prior to the crystal structure determination of RCIII, it was not apparent that a third polymorphic form of TZF (bar the 50:50 solid solution) had crystallized, even though crystals with the distinctive parallelogram habit of RCIII had clearly been observed almost two decades earlier (Fig. 3). Several factors are likely to have contributed to RCIII having been overlooked. First and foremost, identifying component TZF phases from PXRD patterns was a challenge due to extreme preferred orientation, a problem exacerbated by shearing of the crystals during the sample preparation for flat-plate PXRD analysis. As each of the RC polymorphs has essentially the same slip planes, the dominant reflections corresponding to the interlayer spacings, in being shared by all three forms, could not

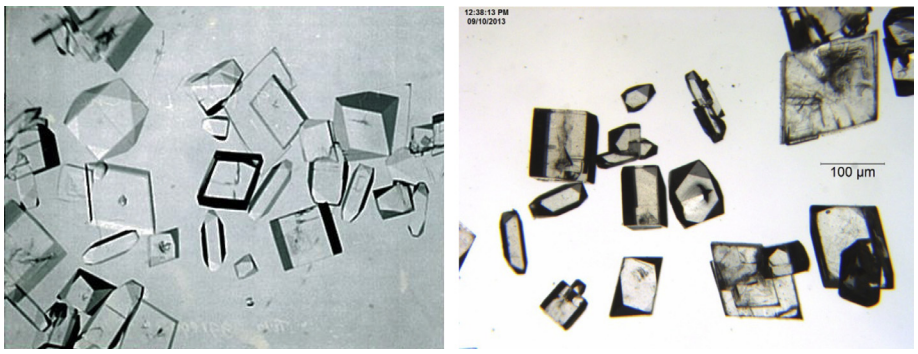

Fig. 3. Photomicrographs of TZF RC crystals grown from toluene in 1996 (left) and after 17 years of storage at room temperature (right).

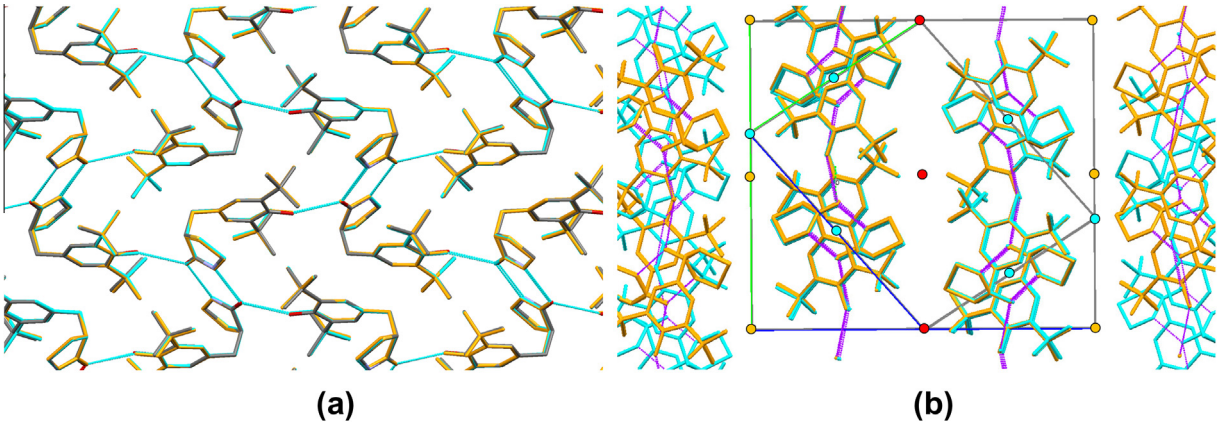

Fig. 4. (a) Overlay of the common layer in RCII (coloured by element), RCI (orange) ($RMSD_9$ of RCI:RCII = 0.117 Å) and RCIII (cyan) ($RMSD_9$ of RCIII:RCII = 0.113 Å) using the 100 K structures. (b) Overlay of RCI (orange) and RCIII (cyan), including the two common layers in the middle of the figure, which give rise to the structures having an $RMSD_{14}$ of 0.061 Å, and the different stackings on either side. The inversion centres that are in common to the two structures are shown in red, while those that appear in only one structure are coloured the same as the atoms of the structure. The cell axes are in the same colours for the two structures.

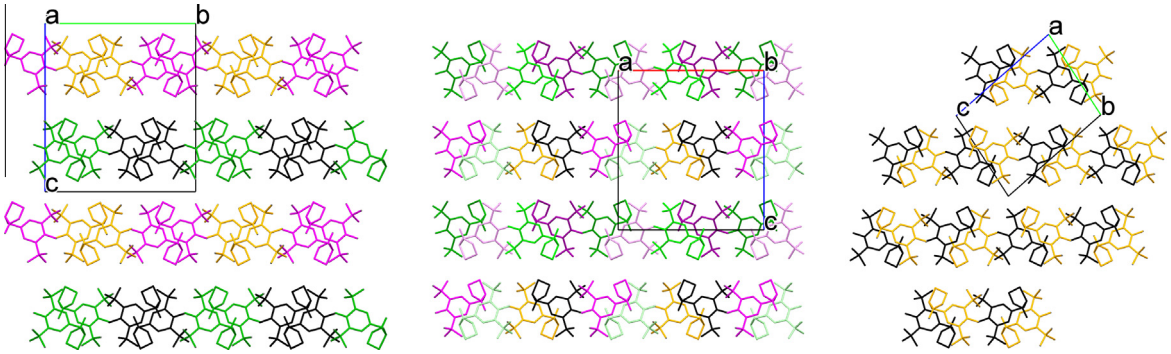

Fig. 5. The symmetry relationships in (left to right) RCI, RCII and RCIII, with the asymmetric unit and its translation related molecules in black, inversion related molecules in orange, 2-fold screw related molecules in green and glide-plane related molecules in pink (in RCII, the three different shades of green and pink mark the three distinct screw- and glide-related molecules). The vertical stacking direction is [001] in RCI, [001] in RCII and approximately [011] in RCIII, as shown by the cell axes.

be used to uniquely identify any of them (Fig. 6). Furthermore, the RCI and RCIII materials that typically crystallized under kinetic conditions did not diffract particularly well, with the weak, but diagnostic, reflections often appearing to be 'smeared'. Spectroscopic techniques were also used to characterize the TZF crystal forms, but were not sufficiently discriminative. FTIR spectroscopy, for example, could not distinguish between RCI and RCII, let alone suggest the possibility of additional forms [13]; solid-state ^{13}C NMR spectroscopy was well-suited for identifying RCII, but was unable to differentiate RCI and RCIII (Fig. 7). Finally, early thermal analysis produced far from conclusive evidence of a third polymorphic form in microcrystalline TZF materials as will be discussed. Without clear evidence from PXRD, FTIR, ssNMR or thermal analysis of another form being present, the diverse morphologies observed in the early batches of single crystals were basically dismissed once the crystal structures of RCI and RCII were solved. Admittedly, RCIII might have similarly been missed in this investigation had RCI and RCII crystals first been chosen for the structure re-determinations.

The intention of this combined study was to extend the experimental enthalpy estimates and errors to lower temperatures to calibrate the computational methods. Accurate DSC measurements were therefore made on freshly crystallized RCI and RCII materials (before the discovery of RCIII) only to find that the previously-reported melting temperatures and enthalpies could not be reproduced. Curiously, further attempts to obtain phase-pure samples lead to even greater variations in the melting temperatures and heats of fusion of seemingly well-crystallized TZF materials (Supplementary Data Section 1.3). Certainly concomitant crystallization of two (or more) polymorphic forms, which proved difficult to avoid with TZF, could contribute to the variable melting behaviours observed for the polycrystalline materials. Therefore, to accurately measure the melting temperatures and enthalpies of RCI–III, avoiding uncertainties due to particle-to-particle heterogeneity, DSC was conducted on single crystals which could be grown large enough to be sorted by hand and analyzed individually. The variability in the DSC results was not improved, however, through this exercise. Not only were the melting transitions fairly broad considering the nature of the samples, but in some cases, multiple, partially resolved melting events were also observed (Fig. 8). Barring any material changes induced by heating, the DSC data provided an initial indication that the TZF 'single crystals' themselves were heterogeneous.

Much of the single crystal DSC data, in showing signs of multiple thermal events, proved unsuitable for determining the melting temperatures and heats of fusion of RCI–III. However, the most homogeneous, i.e., structurally pure, of the single crystals did produce single, reasonably sharp endotherms (coloured traces in Fig. 8), which clustered around three different temperatures corresponding roughly to the melting points of RCI–III. The lowest melting single crystalline form (T_m = 154.6 °C) was assigned to RCII based on the comparable melting point of microcrystalline RCII

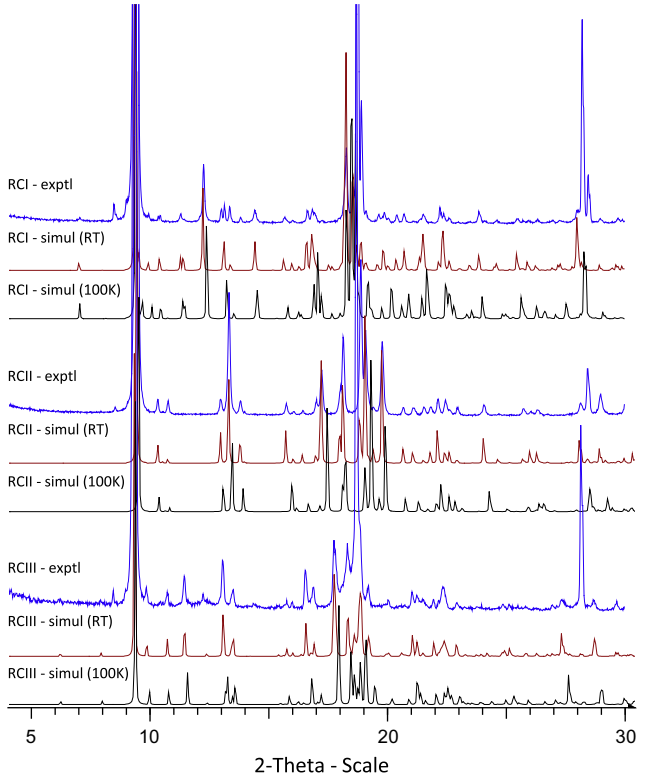

Fig. 6. Experimental and simulated (100 K and RT) PXRD patterns of TZF RCI–III. The small peaks at 8.4° in the experimental PXRD patterns are due to the $K\beta_1$ component of the Cu radiation for the main interlayer reflection.

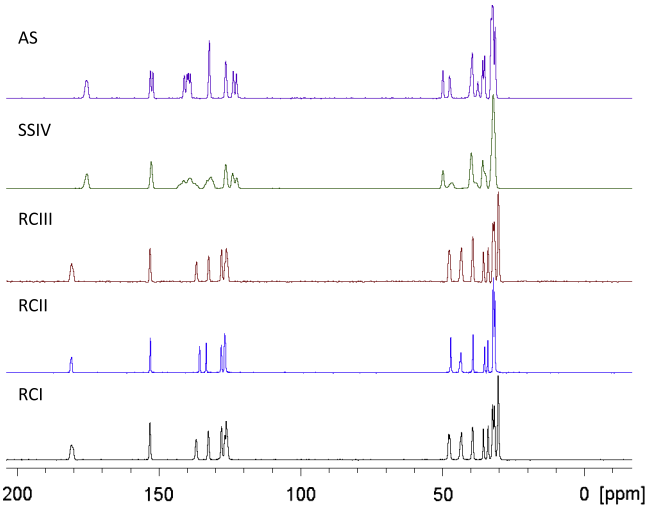

Fig. 7. ^{13}C CP/MAS NMR spectra of TZF crystal forms.

obtained by slurry conversion. RCI (T_m = 158.3 °C) was confirmed as the highest melting form based on the characterization of two identical single crystals grown from the same batch, with one crystal having been indexed to the RCI cell and the other having been shown by DSC to be the high melting form. RCIII (T_m = 155.6 °C) was independently assigned by comparison to DSC data collected for polycrystalline materials that had been identified as RCIII by PXRD. Here, it should be noted that while the melting point of RCII was in fair agreement with the previously reported value [13], the melting temperature of RCI observed by single crystal DSC (this work) was found to be significantly higher and neither melting

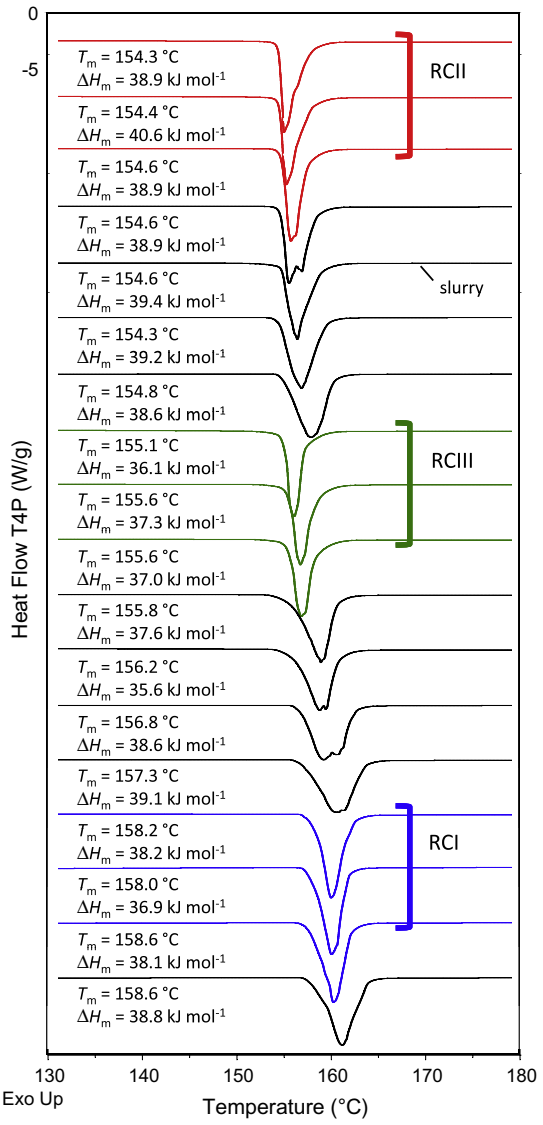

Fig. 8. Melting behaviour of racemic TZF single crystals, along with polycrystalline RCII generated by slurry conversion, roughly ordered by onset temperature. The coloured braces denote the single crystals that from this thermal data appear to be the most structurally pure of those analyzed. DSC curves were measured at 10 °C min^{-1} with a precision of (±0.1 kJ mol^{-1}, ±0.1 °C). Previously reported values are RCI: 156.6 °C, 37.8 kJ mol^{-1}, RCII: 154.7 °C, 39.2 kJ mol^{-1} [13].

enthalpy was in particularly good agreement with those reported in the original work. The discrepancies between the two studies are at least partially explained by the coexistence of RCIII in the original materials, which was clearly not appreciated at the time. Taking RCIII into account, the melting order of the racemic TZF polymorphs is: RCI > RCIII > RCII and the rank order of melting enthalpies is: RCII > RCI ~ RCIII. Thus, RCII appears to be enantiotropically-related (more stable below the thermodynamic transition temperature) to both RCI and RCIII, and RCI appears to be monotropically more stable than RCIII. While their enantiotropic stability relationship to RCII is reasonably certain, RCI and RCIII could only be tentatively assigned without the assurance of having been isolated as structurally-pure single crystals as having a monotropic stability relationship to one another.

TZF had, until the single crystal DSC experiments, appeared to be a relatively straightforward case of polymorphism with three well-defined and crystallized RC structures. The mixed melting behaviours observed by single crystal DSC showed, however, that

the system was not as clear cut as first thought. With RCI–III sharing a common layer structure, polytypism, stacking problems or displacement errors during crystal growth would seem likely, if not inevitable, and depending on their frequency, could lead to variability in the DSC data as well as peak smearing in the PXRD patterns. Therefore, to determine if TZF was susceptible to the same layer stacking problems as aspirin [2] and felodipine polymorph II [48], a closer look was taken at the single crystal diffraction data collected for RCI–III at 100 and 296 K. Precession images were reconstructed, which in the b^*c^* planes (Figs. 9 and S4–S6) clearly showed that each of the TZF single crystals was defective. There is diffuse scattering or streaking along the layer stacking directions, which is usually more obvious for the metastable polymorphs RCI and RCIII. Discrete sets of additional sharp Bragg reflections were observed in the CCD frame data of all of the freshly-crystallized racemic polymorphs, as well as the aged RCII crystal. Interestingly, the additional diffraction peaks were less pronounced in the precession images of the aged crystal than in the freshly grown crystals, suggesting that over time it may have partially self-corrected to the most stable structure. However, even this crystal, which shows the least evidence of disorder of the several RCI–III crystals examined (Figs. S4–S6), shows far more streaking than a precession image from an AR crystal (Fig. S8).

Defective crystals can arise from a variety of sources, such as high thermal motion accompanied by diffusion or structural disorder in the form of stacking faults, dislocations, domains, polytypism or twinning [49]. For RCI–III, having ruled out satellite crystals as a possible source of diffraction, the sets of Bragg reflections observed for several crystals at both 100 and 296 K (Figs. S4–S6) suggested the possibility of intergrowths or domains of alternative RC stackings within the single crystals. Some of the domains may have a twinning relationship; however, the errors observed by diffraction with 'disagreeable' reflections showing $F_c > F_o$, not to mention the variability seen by single crystal DSC, cannot be from twinning alone [50]. Unfortunately, the structurally-characterized racemic polymorphs, while presumed to be among the intergrowths based on the DSC observations, were not identified unequivocally as the minor component phases from the diffraction patterns. This is partly because more than two partially overlapping reciprocal lattices, including misaligned variants of the primary component, were identified in the merged precession images of each single crystal (RCIII example in Fig. S7). Interpretation of the RCI and RCIII diffraction data was further complicated by the considerable streaking between the Bragg peaks, a sign of structure modulation. The single crystal diffraction of RCI–III will be the subject of future investigation; however, in showing secondary lattices (and more) coexisting with the main ones from which the RCI–III crystal structures were solved, the frame data has confirmed that the TZF system is inherently prone to making mistakes during crystal growth. Whether the mistakes are few and far between leading to domains or rampant leading to modulated structures or polytypism is a matter of the crystallization conditions, which are likely to change even from the beginning to the end of the crystallization experiment.

The enantiopure forms, AS and AR, were similarly crystallized to provide material for accurate DSC measurements and specifically to grow single crystals of either enantiomorph for a low temperature X-ray structure determination. In contrast to the RC

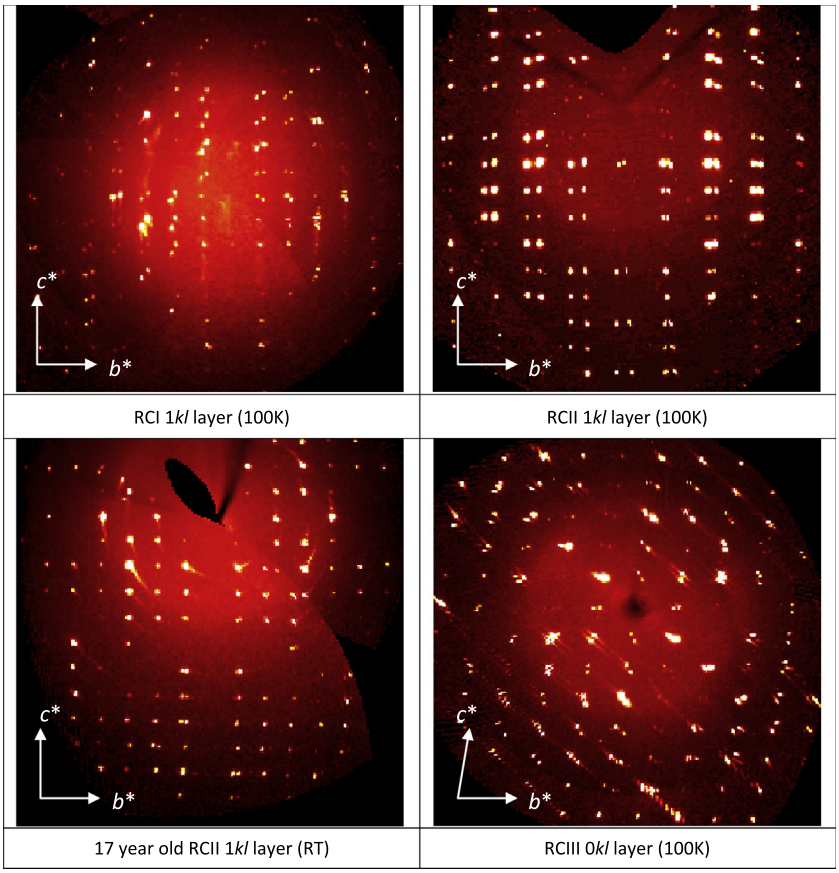

Fig. 9. Reconstructed precession photographs of RCI–III crystals freshly grown from toluene, contrasted with a 17 year old RCII crystal. Multiple sets of Bragg reflections correspond to intergrowths or domains of RC polymorphs; streaks coincide in reciprocal space with the layer stacking directions and indicate a distribution of disorder (layer stacking faults).

polymorph mixtures, which were chemically stable, some of the AR and AS materials retained as crystalline solids for more than two decades had significantly degraded. Therefore, recrystallization of the single enantiomer forms was also required for purification purposes. Luckily, the crystallization attempts on limited quantities of the enantiopure materials did yield AR single crystals suitable for 100 and 296 K structure determinations, along with chemically and physically pure microcrystalline AS.

Apart from their opposing chirality, the AR and AS enantiomorphs were identical as shown by the excellent agreement between the experimental AS and simulated AR (from the 296 K crystal structure) PXRD patterns, Fig. 10. Thus, either AR or AS could be and were used to induce the isostructural solid solution, SSIV, to crystallize from supercooled racemic melts, seeded at 140–145 °C (Table S2). The overwhelming structural similarity between AR (or AS) and SSIV, while readily apparent by PXRD, was further revealed by the comparable chemical shifts at which ^{13}C peaks were observed in their ssNMR spectra (Fig. 7). A notable difference was observed, however, in the ssNMR, and to a lesser extent PXRD, linewidths with the SSIV peaks appearing to be appreciably broadened relative to those of AS. These data suggested that the solid solution might be less crystalline, which would not be altogether surprising as it had been crystallized from the melt, within a period of only 15 min before quench cooling.

Although the crystallinity of SSIV was clearly in question based on the PXRD and ssNMR data, no evidence of either a glass transition or recrystallization exotherm was seen prior to the SSIV melt, as measured by DSC heating at a rate of 10 °C min^{-1} (Fig. S9). In fact, contrary to the previous finding [14] that SSIV partially converted to the more stable RC forms at temperatures as low as 70 °C when heated at 5 °C min^{-1}, the SSIV generated in this study produced a single reasonably sharp melt at 153.4 °C, with a measured enthalpy of 26.9 kJ mol^{-1} (Fig. S9). Although there could be no assurance that the melt crystallized SSIV was 100% crystalline, the contribution of noncrystalline phases to the measured melting point and enthalpy of SSIV appeared to be minimal. The thermal parameters measured for freshly recrystallized AS (149.6 °C, 25.8 kJ mol^{-1}) were in considerably better agreement with the previous determination [13] than for RCI and RCII, although different impurities accumulated over two decades and incompletely rejected during recrystallization seem likely to have contributed to the 1 °C lower melting temperature of AS observed in this work.

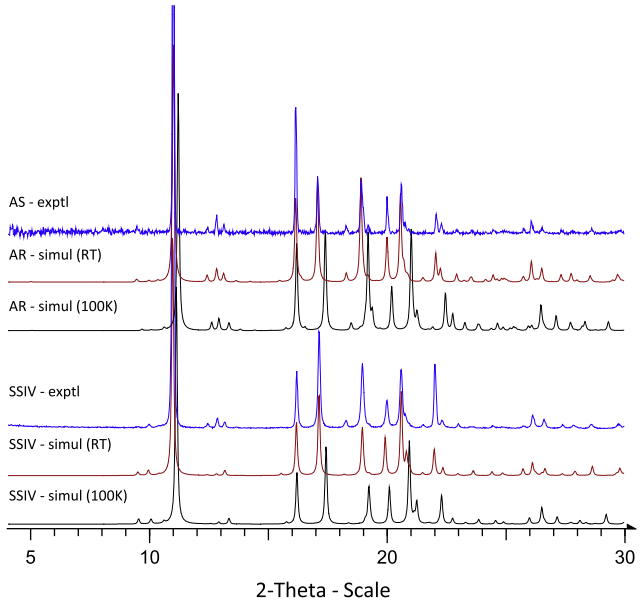

Fig. 10. Experimental and simulated (100 K and RT) PXRD patterns of TZF AR/AS and SSIV.

3.2. Computational reproduction of known crystal structures and thermodynamic stability

There are three main conformational energy minima for an isolated TZF molecule (A, F and C; Fig. 11) in the large region of conformations covered in the search (Supplementary data Section 3). Optimisation of conformation B, which is observed in many structures, results in conformation A as there is no barrier for rotation about C5—C4 so they are in the same conformational well (Supplementary data Fig. S11). One conformational well, C, is not observed in any known crystal structure, but needed to be considered in the search as only slightly higher in energy than conformation B. There are multiple low energy wells within each structural type corresponding to different hydroxyl, methyl or t-butyl angles. The relative energies of the different molecular conformations differ considerably because conformational energies are sensitive to method and basis set due to the variable modelling of intramolecular dispersion (absent from RHF calculations) and intramolecular basis set superposition error [51,52].

The relative lattice energies of the experimentally observed crystal structures, minimized with various methods, are summarized in Fig. 12 (more details in Supplementary data Section 2). All lattice energy minima were in good or reasonable agreement with the experimental structures, with the worst agreement being for the two components of the solid solution, as seen in Fig. 13. However, the relative lattice energies of the structures do vary (as shown in Fig. 12) with the quality of the wavefunction and whether they were calculated for an isolated molecule or within a polarizable continuum. Comparing the 0 K static lattice energies with enthalpies of fusion, by assuming that the enthalpy curves remain parallel over about 430°, would be questionable for monotropically related structures with such anisotropic thermal expansion, even without the sample dependent variations in melting enthalpies (Fig. 8) and the crude approximation to the disorder in the solid solution. The CrystalOptimizer refined structures using the PBE0 intramolecular energy and derived multipoles most closely follow the energy ordering given by the melting enthalpies (Fig. 12) and give marginally better $RMSD_{15}$ overlaps (Fig. 13 and Supplementary data Section 2) with the experimental structures than the other levels of theory tested. Hence this model was used for the final refinement of the lattice energies in the search. The stability order of the experimental ordered structures was incorrect when the intramolecular energy penalty was calculated at the RHF level due to both errors in the relative conformational energy (Fig. 11), and from the description of the intermolecular electrostatic interactions.

3.3. Crystal energy landscape

The $Z' = 1$ search has found the structure RCII as the most stable structure, with an $RMSD_{15}$ of 0.142 Å with the new 100 K redetermination. The minor component of the solid solution, SSIV-B, was found as the second most stable structure with an $RMSD_{15}$ of 0.381 Å with the minor component of the 100 K structure of WIMBAV07, and the major component SSIV-A was also found, a little higher in energy, with an $RMSD_{15}$ of 0.378 Å with the major component. The lattice energy minima for RCI and RCIII (both are $Z' = 2$ experimental structures that could not have been found in the search [53]) are slightly less stable than SSIV-B. Thus all the known racemic structures are found within an energy range of about 5 kJ mol^{-1}, although there are other unobserved racemic structures within this range. These structures are discussed according to their

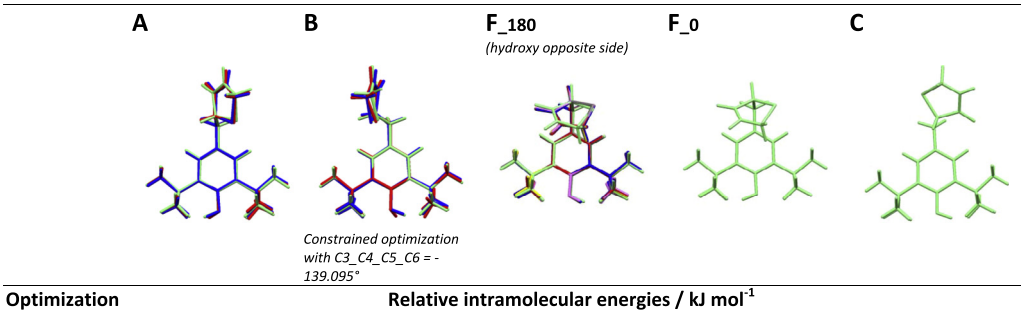

Optimization method	Relative intramolecular energies / kJ mol^{-1}				
PBE0	3.43	8.27	0.50	0	9.85
B3LYP	0.50	5.11	0.60	0	6.18
RHF	0.93	7.34	0.92	0	7.24

Fig. 11. Overlays of the PBE0/6-31G(d,p) ab initio optimized minima (light green) and the similar conformations observed in experimental crystal structures ($RMSD_1$ is for all non-hydrogen atoms), labelled by search region. Region A: AR (red, $RMSD_1$ = 0.118 Å) and WIMBAV07 major component (SSIV-A, blue, $RMSD_1$ = 0.162 Å), Region B: AR (red, $RMSD_1$ = 0.170 Å) and WIMBAV07 minor component (SSIV-B, blue, $RMSD_1$ = 0.228 Å); Region F: RCII (red, $RMSD_1$ = 0.203 Å), the two molecules in RCI (blue, $RMSD_1$ = 0.208 Å, and grey, $RMSD_1$ = 0.177 Å) and the two molecules in RCIII (pink, $RMSD_1$ = 0.205 Å, and yellow, $RMSD_1$ = 0.179 Å). The hydroxyl proton position is defined by the C7_C8_O2_H torsion angle. If the conformations are optimized with B3LYP/6-31G(d,p) or RHF/6-31G(d,p) the structures are visually indistinguishable, but the relative energies differ.

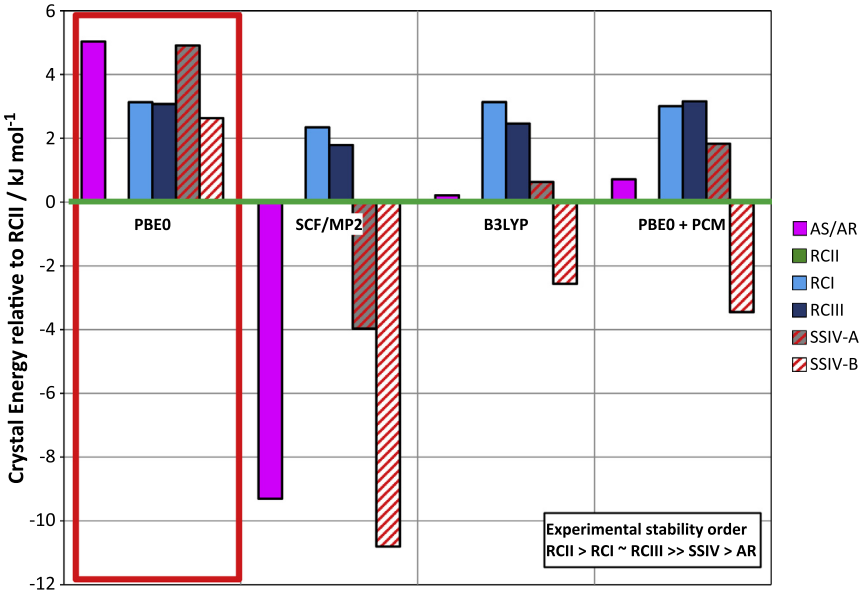

Fig. 12. Lattice energies of the various crystal structures relative to RCII. Each dataset is labelled by the level of theory used to evaluate the intramolecular energy and molecular charge density (where only one level of theory is given, the same is used for both calculations). PCM indicates that the wavefunction was calculated in a polarizable continuum with a relative dielectric of 3. The 6-31G(d,p) basis set was used in all cases. The PBE0 method (highlighted in red) was used in the search.

hydrogen-bonding graph set classification below (see Supplementary data Fig. S12 for further details).

The Z' = 2 structure of the enantiopure crystal (AR) is higher in energy than the layer based racemic structures RCI–III, and comparable in energy with the less stable solid solution component. However, it is 6 kJ mol^{-1} more stable than all other enantiopure structures generated in the search (Supplementary data Section 4.3).

3.4. Structures containing the F conformation with $R_2^2(8);C_1^1(10)$ hydrogen bonding, including RCI–III (green squares on Fig. 14)

All of the structures with this motif below −130 kJ mol^{-1} on Fig. 14 (further details in Supplementary data Section 4.4) form the same sheet observed in RCI–III of molecules in the folded F conformation, connected by $R_2^2(8)$ head-to-head amide-amide interactions, cross-linked by $C_1^1(10)$ hydroxyl-carbonyl interactions. There are four unobserved, computer generated structures within 7.5 kJ mol^{-1} of RCII that contain this sheet. Three of the daughter structures have a stacking qualitatively related to RCI and RCIII and close in energy to them (TZF9223, TZF9837 and TZF13647 on Fig. 14), while the fourth, TZF28134, has the stacking mode that is found in RCII (Fig. 5 and Supplementary data Fig. S17), but is comparatively higher in energy. The relationship between the stacking and powder patterns of the computer generated and observed layer structures is illustrated in Supplementary data (Figs. S17, S19 and S20).

3.5. AR/AS, the solid solution, and other structures containing the AB conformation with $R_2^2(6)$ graph sets (blue circles on Fig. 14)

The experimentally observed enantiopure crystal structure, AR or AS, has its two molecules in the extended conformations A and B (hence Z' = 2) with the $R_2^2(6)$ hydrogen bonding motif

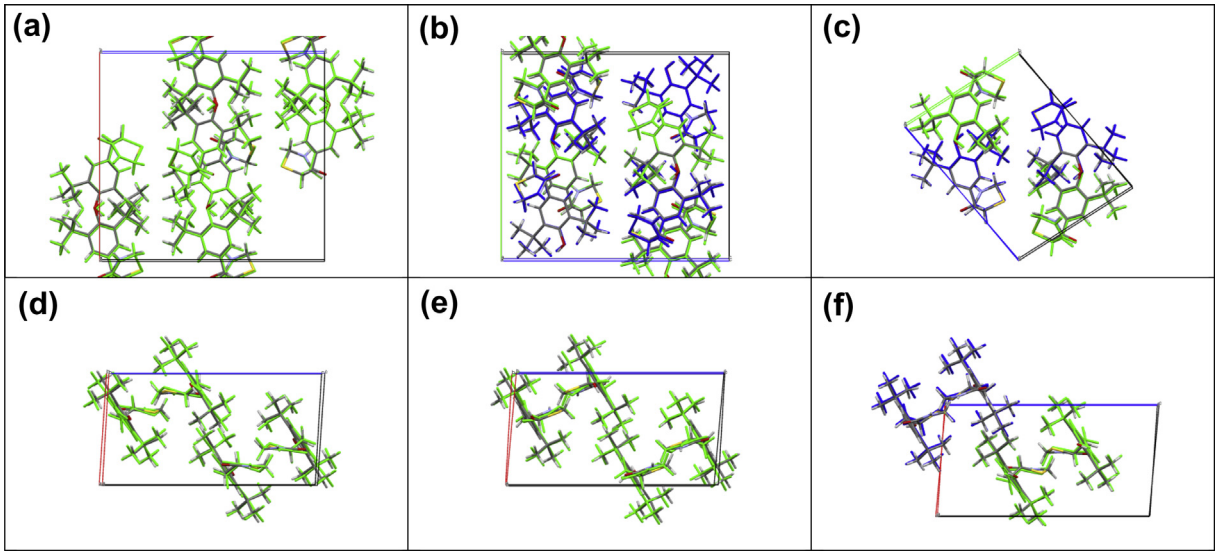

Fig. 13. Overlay of experimentally determined structures (coloured by element) with the computational model structures, i.e. the minima in the lattice energy for the model used in the search (coloured by symmetry equivalence). (a) RCII ($RMSD_{15}$ = 0.141 Å with 100 K structure), (b) RCI ($RMSD_{15}$ = 0.162 Å with 100 K structure), (c) RCIII ($RMSD_{15}$ = 0.148 Å with 100 K structure), (d) WIMBAV07 major component SSIV-A ($RMSD_{15}$ = 0.238 Å), (e) WIMBAV07 minor component SSIV-B ($RMSD_{15}$ = 0.346 Å), and (f) AR ($RMSD_{15}$ = 0.216 Å with 100 K structure).

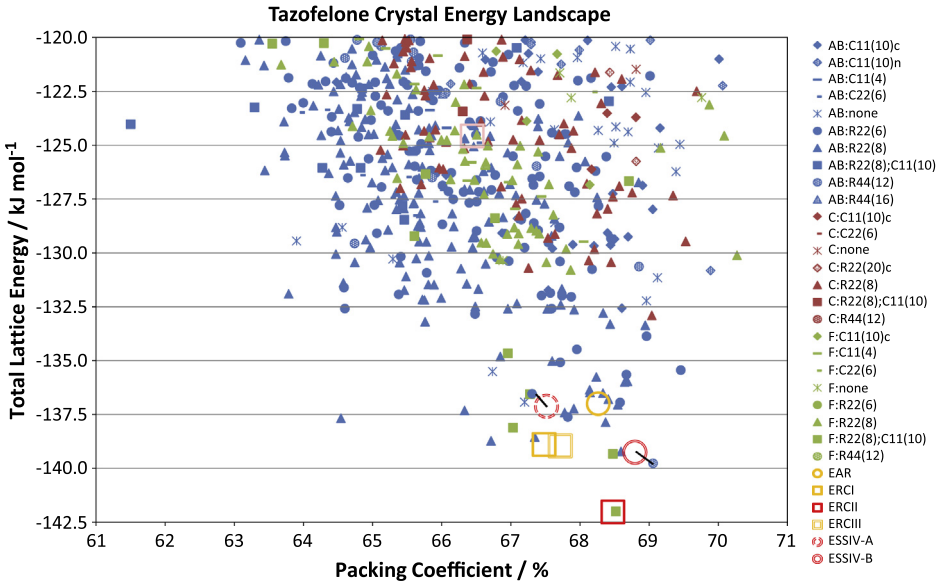

Fig. 14. Summary of the CSP study of TZF. Each point represents a lattice energy minimum, with structures categorized by colour to denote the type of conformation (AB is the large conformational region of extended molecular structures, F is the folded conformation, C is another low energy conformation, (Fig. 11)) and symbol to denote the hydrogen bonding graph set. Open symbols denote the corresponding lattice energy minima for the experimental structures, which are orange for Z' = 2 structures which could not be found in the search. All experimental Z' = 1 structures were found in the search. The structures that matched the two components of the solid solution (ESSIV-A and ESSIV-B) were at slightly different energies, caused by slightly different conformation and associated packing changes – this is indicated on the plot by the black tie-lines. The search generated structures (Supplementary data Table S6) are labelled by TZF*x*, where *x* is the ranking of the structure generated by CrystalPredictor, i.e. with point charges and without conformational refinement. The high energy pink square corresponds to the RCII structure with the hydroxyl proton rotated by 180° as in the CSD entry WIMBAV.

depicted in Fig. 15 between the hydroxyl and the amide group. The molecules thus form chains linked by the hydrogen bonds. The experimental structure is lower in energy than any enantiopure Z' = 1 crystal (see Supplementary data Section 4.3), but the two calculated structures closest in energy (TZF20 and TZF3891) are based on the same $R_2^2(6)$ chains, but with only one conformation (A). Hence, the Z' = 2 distinction of conformations A and B provides a packing of this chain that gives a more favourable energy. All the enantiopure structures within 17 kJ mol^{-1} of AR contain the molecule in the extended conformation (see Supplementary data Fig. S13).

The $R_2^2(6)$ chain of extended (AB) conformations can pack much more effectively in racemic space groups than in an enantiomorph such as AR/AS. This includes the solid solution (SSIV) structures, though in SSIV-B, molecules in the two $R_2^2(6)$ chains have twisted so that the oxygens within different chains are within a short contact distance giving an $R_4^4(12)$ motif. Thus the crystal energy landscape has shown the existence of racemic structures closely related

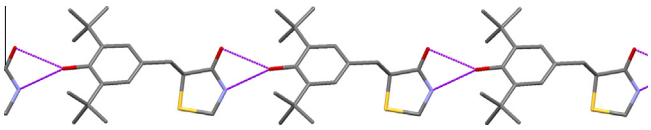

Fig. 15. Hydrogen bonding in the $R_2^2(6)$ motif.

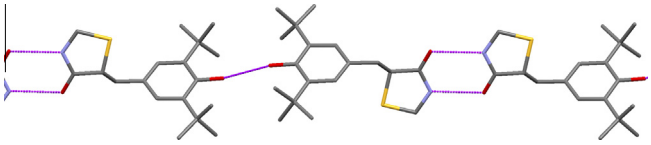

Fig. 16. The AB:$R_2^2(8)$ amide dimer showing a tail-to-tail interaction of the hydroxy group in structure TZF1481 (-137.673 kJ mol^{-1}).

in the dominant packing motif to the AR/AS structure, but lower in energy. So when both enantiomers are present, the chain packing of the enantiopure AR/AS structure can be formed, though the alternative layer packings of RCI/RCIII and RCII are competitive or more stable, respectively.

3.6. What other solid state motifs are energetically feasible?

Although the C conformational region is energetically competitive in the gas phase, the molecule appears not to be able to pack effectively with this conformation in crystal structures. The most favourable packing is 9 kJ mol^{-1} above the global minimum energy structure, and is higher in energy than all of the experimentally observed forms. Thus all low energy structures are in the low energy conformational area that spans the extended and folded structures (Fig. 11 and Supplementary data Fig. S11).

The study has generated many crystal structures which have the molecules linked by the amide groups forming a doubly hydrogen bonded $R_2^2(8)$ dimer. However, these structures are only thermodynamically competitive with the observed racemic forms when the molecules are in an extended AB conformation (blue triangles on Fig. 14). In many cases there is no conventional hydrogen bonding interaction of the hydroxyl group with a neighbouring molecule, though a few very high energy structures (~ -128 kJ mol^{-1}) form a hydrogen bond of the hydroxyl group to the carbonyl (the AB:$R_2^2(8)$;$C_1^1(10)$ blue squares on Fig. 14). The majority of structures with the AB:$R_2^2(8)$ amide dimer have a tail-to-tail interaction of the hydroxy group with another molecule as shown in Fig. 16.

4. Complementary analyses: hydrogen bonding

To the extent that hydrogen bond donor and acceptor participation and favourable (or otherwise) donor–acceptor pairings can be used to rationalize form stability, the experimental and low energy calculated TZF structures were compared using the Cambridge Crystallographic Data Centre Hydrogen Bond Propensity (HBP) tool [45] (Supplementary data Section 5.1). The HBP results based on modelling of two donors and three acceptors in TZF are shown in Table 2, with the difference in the competition factor between $Z' = 1$ and $Z' = 2$ structures resulting in a small spread of propensities. Of the donor–acceptor pairings, the hydrogen bond with the highest propensity to form was the N—H···O interaction between the amide N and O of near neighbours. This highest probability interaction was observed in the racemic polymorphs, RCI–III, but not in the single enantiomer structure (AR). The next most abundant interaction, the O—H···O hydrogen bond formed between the aromatic OH and the amide O, is present in each of the structures; however, the propensity to form the N—H···O hydrogen bond needed to close the $R_2^2(6)$ ring in the homochiral crystal structure appears to be relatively low.

The propensity results correlate reasonably well with the observed AR structure being less stable than the racemic structures. The crystal energy landscape has further shown that it appears not possible for the enantiopure structure to adopt a more stable polymorph with the highest propensity hydrogen bond. Thus in cases where the stable form is desired, but a relatively quick HBP analysis shows that the known structures do not have the highest propensity hydrogen bond, the experimental search for such polymorphs could be reduced by calculating the more molecule-specific crystal energy landscape if this showed that the higher propensity interactions are not represented among more stable structures. For TZF, racemic CSP structures that are more stable than AR (Fig. 14) do in fact have the hydrogen bonding motif AB:$R_2^2(8)$ with the highest propensity amide N to amide O hydrogen bonds, but are unobserved. Additionally, two racemic structures (TZF529 and TZF844) that are only marginally less stable than the observed racemic polymorphs do not have any conventional hydrogen bonds, but instead a variety of short contacts, such as amide N—H to aromatic phenyl rings. These examples emphasize the limitations of "counting hydrogen bonds" relative to the stabilization from the many interactions involved in close packing molecules in low energy conformations.

How well do the observed interactions in the experimental TZF structures conform to the expected donor and acceptor positions derived from similar molecules? Insights into the 'quality' of the hydrogen bonding interactions were provided by FIM [46] visualization of the interaction preferences in relation to the hydrogen bonding groups of near neighbour TZF molecules. The FIM results (Fig. 17 and Supplementary data Section 5.2) complement the HBP analysis (Table 2), taking into account the geometry of the hydrogen bonding interactions, not simply the number of used and unused donors and acceptors. Extending the TZF FIMs to H-bonded molecules has shown that even for the RC polymorphs,

Table 2
Hydrogen bond propensity analysis of TZF racemic and homochiral crystal forms. The bold variables highlight the slightly different hydrogen bond propensity values calculated for the $Z' = 1$ and $Z' = 2$ structures resulting from different competition factors.

Donor	Acceptor	Donor steric density	Acceptor steric density	Donor/acceptor aromaticity	Competition ($Z' = 1$)	Propensity ($Z' = 1$)	Upper/lower bound ($Z' = 1$)	Competition ($Z' = 2$)	Propensity ($Z' = 2$)	Upper/lower bound ($Z' = 2$)	Observed
Amide N	Amide O	38.75	38.45	0.30	2.0	**0.84**	0.74/0.90	4.0	**0.81**	0.70/0.89	RCI, RCII, RCIII
Hydroxy O	Amide O	68.55	38.45	0.30	2.0	**0.54**	0.39/0.69	4.0	**0.50**	0.35/0.66	RCI, RCII, RCIII, AR
Amide N	Hydroxy O	38.75	68.55	0.30	3.0	**0.13**	0.07/0.25	6.0	**0.11**	0.05/0.21	AR
Amide N	Thioether S	38.75	48.31	0.30	3.0	**0.09**	0.06/0.13	6.0	**0.07**	0.05/0.11	AR
Hydroxy O	Hydroxy O	68.55	68.55	0.30	3.0	**0.03**	0.02/0.07	6.0	**0.03**	0.01/0.06	
Hydroxy O	Thioether S	68.55	48.31	0.30	3.0	**0.02**	0.01/0.03	6.0	**0.02**	0.01/0.03	

No intra-molecular hydrogen bonds predicted (using pre-defined model).

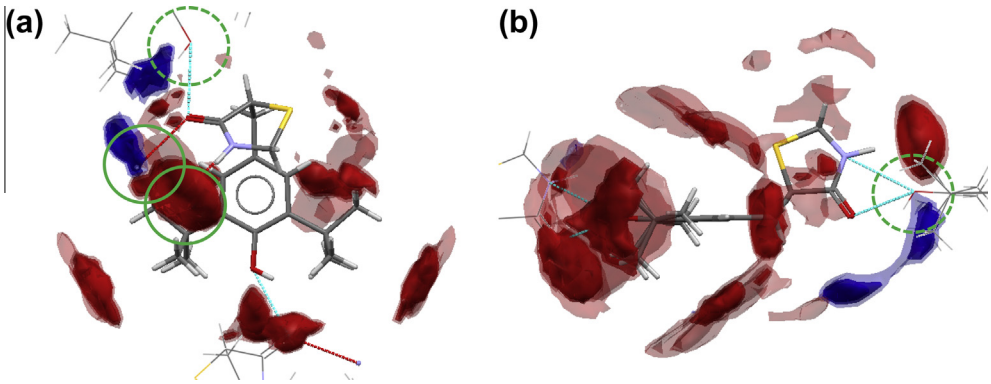

Fig. 17. Full Interaction Maps (FIMs) of TZF molecules as packed in the (a) RCII (identical H-bonding to RCI and RCIII) and (b) AR (identical to AS and SSIV) structures. Green circles highlight hydrogen bonding that satisfies (solid) and does not satisfy (dotted) donor and acceptor hotspots surveyed using carbonyl O acceptor (red) and uncharged NH N donor (blue) probes.

where the H-bond propensity of the carbonyl group appears to be satisfied (by two interactions), the geometry of the second interaction (dotted green circle shown for RCII on Fig. 17a) is not well represented in the statistical analysis of the CSD entries. For the extended TZF molecules in AR, none of the donor and acceptor hot spots near the lactam ring in the contour maps appear to be particularly well occupied (Fig. 17b). The Full Interaction Maps give a useful guide to highly likely interactions, but some are misplaced, as the close packing principle leads to considerable compromises involved in trying to pack the molecule without high energy conformational distortions. This type of analysis is also complementary to the CSP, which in the lattice energy is balancing the strength of all molecule specific intermolecular interactions, including those that favour the close packing of molecules, with the conformational flexibility of the molecule. This leads to the specific compromises seen in the low energy structures.

4.1. Hydroxyl involvement in stabilizing crystal structures

Hydrogen atom positions are often not determined from X-ray diffraction data, but their positions are critical to the relative stability of structures, particularly for forming hydrogen bonds. This is illustrated by the lattice energy minimum corresponding to the CSD entry WIMBAV [13], which has the hydroxyl proton position rotated by ~180° relative to the 100 K structure of RCII, being found in the search 17 kJ mol^{-1} higher in energy than RCII (Fig. 14) as the $C_1^1(10)$ hydroxyl and carbonyl interaction is missing. This large energy difference shows that the hydroxyl proton is not sterically hindered by the t-butyl groups, but is capable of forming strong hydrogen bonds as found in all the experimentally observed structures. Furthermore, our initial lattice energy optimization starting from the WILZUM structure, which has the hydroxyl protons coplanar with the aromatic rings, instead of the 100 K redetermination of AR, resulted in a poorer reproduction of the crystal structure because the molecule in conformation B needs to distort to achieve a favourable interaction with the misplaced proton, with an energy approximately 2.5 kJ mol^{-1} higher (Supplementary data Fig. S13). This further illustrates the value of computational minimization of crystal structures with a variety of starting proton positions to highlight incorrect hydrogen atom placements [54–56].

Analysis of phenol structures in the CSD, comparing hydroxyl conformations and the effect of adding t-butyl groups on either side (Supplementary data Section 5.2), suggests that the t-butyl groups lead to a higher proportion of out of plane OH protons. While the phenol OH is a reasonably good hydrogen bond donor in any orientation, FIMs constructed for a representative sampling of the variably substituted phenols using a donor probe (see Supplementary data Section 5.2 for details and Fig. S25) show that the probability of the hydroxyl group accepting a hydrogen bond is very dependent on the C—C—O—H torsion angle, increasing significantly as the hydroxyl group is twisted out of the plane of the aromatic ring. For RCI–III, the phenol OH is essentially coplanar with the aromatic ring and this group functions only as a donor (Fig. S24). In contrast, the C—C—O—H torsion angles are about 35° and 65°, respectively, in AR conformers A and B, which donate and accept hydrogen bonds. Clearly, the steric hindrance from the t-butyl groups does not "isolate" the hydroxyl proton, but whether it is forming "hydrogen bonds" is rather dependent on definition. For example, the t-butyl/hydroxyl tail-to-tail interaction (Fig. 16) would appear to be stabilizing the unobserved AB:$R_2^2(8)$ motif (i.e. the less stable conformation's ability to pack with amide hydrogen bond dimers). This motif does appear in other structures on the CSD, Supplementary data Table S7. However, it is not possible to distinguish the stabilization afforded by the weak, low propensity OH···OH hydrogen bond from that provided by interactions involving the t-butyl groups.

5. Discussion

5.1. How does the crystal energy landscape help to understand the solid solution formation?

The observation that there are racemic structures of tazofelone that are isostructural with, but more stable than, the enantiopure crystal suggested the possibility of new racemic forms, different from the more stable sheet packings of RCI–III. Historically, the discovery of the solid solution (including the 50:50 racemic polymorph SSIV) came from exploring the phase diagram of TZF and finding that the mixed melting points of the racemate and enantiomorph showed neither the expected melting point depression nor eutectic melting. The solid solution was later prepared by seeding a racemic melt with enantiomorph crystals, with powder diffraction confirming that the crystallites that grew from the seed were isostructural with it. Experience of cross nucleation [15] had suggested that seeding the supercooled racemic melt might promote nucleation of this new phase, disrupting crystallization of the more stable forms RCI or RCII. Since then, there has been an increased appreciation of the role of templates or pseudoseeds in nucleating new forms [57], such as catemeric carbamazepine form V [58], the photostable cocrystal of photoactive resorcinol [59], or the caffeine:benzoic acid cocrystal [60]. Hence the energetic and structural relationship between the racemic AB:$R_2^2(6)$ low energy structures and the enantiopure AR/AS structure would suggest that attempting seeding experiments might be worthwhile.

Further attempts to make the racemic polymorph SSIV from the melt have only been successful when seeded with AR or AS. Hence, it is likely that seeding is required to provide a heterogeneous nucleation pathway for the $P2_1$ AB:$R_2^2(6)$ structure when the presence of both enantiomers means that it is in competition with nucleation and growth of the layer structures containing the more stable conformation and more probable amide hydrogen bonding of the RCI–III polymorphs. Thus, SSIV clearly demonstrates that crystal energy landscapes have the potential to suggest unconventional crystallization experiments to find further forms, and current work aims to develop the ability to find templates to realize computationally predicted polymorphs.

5.2. How does the crystal energy landscape help understand the problems in obtaining phase pure racemic crystals?

This study has revealed that obtaining phase pure TZF samples by normal standards of measurement (excellent match to simulated PXRD patterns, sharp DSC melts, ssNMR spectra, etc.) does not ensure that well-grown single crystals are structurally pure, as shown by inspection of the precession data. There is a degree of structural variability within the single crystals of RCII (and RCI and RCIII) as although some had a sharp DSC melt others did not (Fig. 8), and the raw diffraction data varied with the single crystal (Figs. S4–S6). X-ray powder diffraction of samples obtained by crystallizing racemic mixtures almost always featured the (002), (004) and (006) reflections in common to RCI and RCII, as expected from the interlayer spacing. Sometimes these were the only sharp peaks observed, consistent with layer stacking issues. The shearing of the crystals exacerbated already strong preferred orientation effects further reducing the ability of X-ray diffraction to determine the structural purity of the samples. With care, apparently phase pure RCII can be obtained, but the XRPD patterns and thermal measurements on RCI samples showed far too much sample dependent variation. The existence of other layer structures on the crystal energy landscape close in energy and structure to RCI, with the same layer as RCII, suggested that this may be caused by either stacking disorder or further closely related polymorphs. The discovery of RCIII single crystals by manual inspection of samples of "RCI" confirmed that there is at least one further polymorph, albeit one with great similarity in packing (Fig. 4) and energy (Fig. 12, Supplementary data Table S5). In this instance, minimal structural discrimination [49] in terms of symmetry (Fig. 5), intermolecular distances and energy lead to defining the two structures as polymorphs rather than sample dependent variations. There were also sample dependent variations as shown by examination of the diffraction images from various single crystals (Fig. 9) exhibiting a very high mosaicity, consistent with there being a small domain size and misalignment of the domains. There was some evidence of structure modulation along the layer stacking direction, possibly incommensurate or polytypism, suggesting that understanding organic modulated crystal structures [61] is of relevance to pharmaceutical development. The evidence of disorder in the single crystals has to be contrasted with sharp NMR peaks which implies local order. Hence, it is clear that these samples are not structurally pure in that all types of defects and disorder are not distributed homogeneously among the particles [1].

The crystal energy landscape showed that there are alternative ways of stacking the layers of RCII, i.e. generating daughter phase structures, with very similar lattice energies and the same PF. Even if RCI had not been known, there would have been a clear indication of the potential for related "daughter" metastable polymorphs, stacking or other disorder. The different symmetry relationship between the layers in RCII and the closest energy structures indicates a different stacking relationship that once formed as an error in nucleation and growth would be hard to correct. Thus, the existence of an RCI type structure could have been anticipated from the crystal energy landscape. This relationship is consistent with the solid state transformation between RCI and RCII being sufficiently difficult that there are two concomitant melts in the DSC, and the self-correcting transformation of the 17 year old crystal being only partial. The full details of the ($Z' = 2$) structures found for RCI and RCIII could not be anticipated from the crystal energy landscape, but the structural and energetic relationship between TZF9223, TZF9837 and TZF13647 suggests the possibility of concomitant polymorphism, and/or a range of epitaxial relationships or stacking disorders, of structures with essentially the same layers as RCII. Judging by attachment energy calculations (Supplementary data Table S8) on these sheet structures, the sheet surface is the slowest growing, morphologically dominant surface, with an attachment energy of ~ -30 kJ mol^{-1} regardless of the stacking. Thus, both the total lattice energy and the stacking energy of the dominant sheets are very similar between the three polymorphs and some computer generated structures. The weak dispersion interactions holding the layers together in the different stacking modes (Fig. S17) in combination with the flexibility of the sheets themselves explains the ease with which the racemic TZF crystals shear along the slip planes. Whether or not the epitaxial relationship between the layers in the hypothetical structures is part of the mosaic spread of the experimental forms is a matter for conjecture, but their close relationship does illustrate the potential for the lack of structural purity [1] that bedevilled the attempts to obtain phase pure RCI and led to the discovery of RCIII.

5.3. Are there more polymorphs to be found?

As TZF, developed as a racemic mixture two decades ago, has not been subjected to a modern polymorph screen and the solid form landscape of enantiopure TZF is almost unexplored, it is unsurprising that the number of predicted structures exceeds the number of observed racemic and enantiopure polymorphs. In fact, we would expect a CSP study to generate more low energy structures than readily accessible polymorphs. The lattice energy minima on Fig. 14 may not be free energy minima, and the rearrangement of the structure during crystallization means that closely related structures may not be found as polymorphs, though they could be realised as stacking faults or disorder [62]. For TZF, most of the thermodynamically favourable structures have strong similarities to the forms already observed, either being based on the F:$R_2^2(8)$;$C_1^1(10)$ sheet structures of RCI–III, or the AB:$R_2^2(6)$ chains of the solid solution structures and enantiopure forms AR and AS. The main unobserved competitive structures are based on the AB:$R_2^2(8)$ motif having the same amide double hydrogen bond interaction as RCII, but a different conformation which prevents the formation of the —OH···O=C hydrogen bond in the stable sheets. Solution NMR suggested [13] sufficient flexibility between the AB and F conformations that trapping the most stable AB:$R_2^2(8)$ as a growth unit for a metastable polymorph, and preventing it folding over to the F conformation to better satisfy the available hydrogen bond donors and acceptors [63] as in the RCI–III layers, is likely to be difficult. The tail-to-tail interaction, whilst stabilizing this type of hypothetical structure, is unlikely to promote the rapid growth of chains of AB:$R_2^2(8)$ motif and prevent rearrangement to the more stable F:$R_2^2(8)$;$C_1^1(10)$ forms. Thus, the likely ease of conformational change and lack of strong hydrogen bonding to help trap AB:$R_2^2(8)$ structures as TZF polymorphs contrasts with GSK269984B [9], where the question was whether the barriers to conformational change were too high to allow the low energy structures with grossly different conformations to nucleate metastable polymorphs.

In contrast, the crystal energy landscape for just the chiral space groups (Supplementary data Section 4.3) shows that the observed

Z' = 2 AR structure is 6 kJ mol^{-1} more stable than fairly similar structures based on the same motif but just one conformer (Fig. S11). This suggests that there may be the occasional conformational error in the crystal packing, but the conformational flexibility of TZF would generally allow the molecules to form the most stable observed AR structure. The first structure with a different hydrogen bonding motif (TZF3231) contains an AB:$R_2^2(8)$ amide dimer and thus contains the higher propensity hydrogen bond, but packs less densely and is 8 kJ mol^{-1} less stable than the observed form (see Supplementary data Fig. S13) and so is unlikely to be observed.

5.4. Relative stability of crystal structures

Although the ability to calculate the relative lattice energies and conformational energies of TZF has increased significantly since the original force-field study, Fig. 12 shows there is still some way to go for accuracy in thermodynamics. TZF represents a particular challenge, as structures that differ in conformation, hydrogen bonding and van der Waals stacking are competitive in energy, and hence the lattice energy differences are a subtle balance of conformational energy, intermolecular polarization, repulsion, dispersion and electrostatic forces. The enantiotropic relationships of RCII to RCI and RCIII and the anisotropic expansion of the crystals implies that there is significant anharmonicity in the molecular modes, which suggests that a harmonic estimate of the zero-point and thermal energy contributions [64–66] may not adequately capture the energy differences. The intended study of heat capacities would have been very useful in seeing how the relative enthalpies of the crystal forms extrapolated to 0 K, but the problems of structural purity clearly frustrate providing accurate targets for computational chemistry. This study provides a warning of the dangers of trying to produce target datasets for benchmarking computational methods of estimating relative energies of polymorphs without a multidisciplinary approach to checking polymorphic purity.

5.5. Significance in the context of development of pharmaceuticals

Structural purity, i.e. having the same 3D molecular arrangement throughout every particle, is highly desirable, if not essential, for drug substances as fluctuations can lead to inconsistency in physical and chemical properties directly impacting drug product performance [1]. Revisiting TZF in the racemic layer forms, RCI and RCII, has illustrated the problems in ensuring structural purity, with advances in the techniques of physical characterization showing what previously was considered an unproblematic polymorphic pair to instead be a patchwork of heterogeneous domains of at least three alternative layer stackings, including that of newly discovered RCIII. Whereas the stable polymorph, RCII, was produced in phase pure form with relative ease, RCI and RCIII were obtained under kinetic conditions conducive to crystallization of concomitant polymorphs. The difficulty in getting phase pure samples of the two closely related metastable polymorphs, apart from extracting single crystals, is not uncommon for pharmaceuticals, for example forms II and III of olanzapine [10]. However with TZF, errors in crystal growth produced individual crystals that were defective. This investigation gives a molecular picture behind the intrinsic variability that could help to define acceptable processing conditions to target the stable form and rationalize why perfect control over metastable form appearance might not be possible in this case.

The TZF experience also builds on the growing awareness of the issues of crystal disorder, very similar polymorphs and sample dependent properties for industrial solid state development. Carefully investigated small molecule systems have shown, for example, complex behaviour similar to that of SSIV that can arise when different conformations, or in rare cases enantiomers, have a similar steric envelope (c.f. Fig. 2), allowing them to occupy the same crystallographic sites, while preserving the strongest intermolecular interactions. Whereas site disorder may arise from different conformations being simultaneously trapped in the same structure, as found in trospium chloride [67,68] and promethazine hydrochloride [69], the incorporation of the opposite enantiomer in a homochiral crystal structure can lead to a solid solution or pseudoracemate, as in diprophylline [70]. Carvedilol phosphate is a particularly complex system in which both R- and S-enantiomers make multiple conformational adjustments in order to fit in the crystal structure of the solid solution [71]. Structural disorder is, of course, not limited to individual molecules or parts of a molecule; energetically competitive assemblies of one or two-dimensional periodic fragments comprised of sets of molecules can also add to the complexity, with the layer intergrowths and stacking errors of aspirin [2], progesterone in "disappearing" form II [72] and now TZF RCI–III serving as prime pharmaceutical examples.

Distinguishing very similar polymorphic forms from defective or modulated structures is not a trivial exercise and usually requires an understanding of the solid state chemistry at the molecular level that is attainable only through a combination of characterization methods. Computational chemistry, when used in conjunction with diffraction, spectroscopic and thermal techniques, has shown great promise in bolstering experimental efforts to characterize structural purity in pharmaceutical solids. Crystal energy landscapes that show closely related daughter phases containing the same periodic fragment as the most stable mother phase [47] should, for example, prompt consideration of related structures, stacking faults, incommensurate structures or other related disorder. The crystal energy landscape of eniluracil in fact helped rule out polymorphism as the source of structural deviations observed by SXRD, showing instead that different degrees of disorder in the interdigitation and stacking of hydrogen bonded ribbons within the crystal structure accounted for the sample variation [73]. With TZF, RC single crystals were sufficiently phase pure to exhibit unique morphologies (Fig. S1) and they diffracted well enough for a reasonable structure solution and refinement of three distinct polymorphic forms. However, our knowledge from the crystal energy landscape of there being other ways of packing the TZF molecule that are related to RCI–III, coupled with the complexity of the diffraction and thermal data, suggests that we have a system involving more than just similar polymorphs. The molecular picture of the variability in the properties that has emerged is one of intrinsic growth of defective crystals derived from different stackings of the layers in RCI–III and other related structures, which might not have been identified without either the single crystal precession images or the crystal energy landscape with its similar stackings having prompted closer inspection. The structural model explaining the variability in TZF is not as clear-cut as that derived to rationalize the diffuse scattering and variable surface features of phloroglucinol dihydrate [74]. It is more like that of chlorothalonil, where the low energy hypothetical structures helped to explain different types of disorder clearly manifest in crystal structures of two metastable phases and highlighted the possibility of many more related structures within the crystallites [75].

Finally, TZF was developed at a time when it was commonplace to market drugs as racemic mixtures. Today, however, with potentially different pharmacological and toxicological effects of the 'inactive' enantiomer to be considered, TZF would most assuredly be evaluated as the active single enantiomer [76]. Here, it is worth noting that calculating the crystal energy landscape for just the chiral space groups, as might be done when developing a single enantiomer, would have represented a significant saving in computational effort. However, it would have missed revealing the isostructural relationship between the enantiopure and racemic structures that encourages incorporating rather than rejecting

the mirror image impurity. Although some spontaneously resolving chiral molecules have been shown to have very similar, albeit not isostructural, energetically competitive computer generated racemic structures [77], TZF and carvedilol phosphate hemihydrate [71] are clearly unusual in their ability to form a racemic solid solution. As such, calculating the crystal energy landscape of a chiral molecule in all space groups would certainly add to the completeness of the study, though it might be argued that in pharmaceutical development the computational expense incurred would usually be better directed to generating other higher probability, but equally important structures ($Z' > 1$ polymorphs, hydrates, etc.) in chiral space groups only.

6. Conclusions

The solid state of TZF is complicated, showing two types of disorder: in addition to the previously reported solid solution, we have found problems in producing phase pure microcrystalline samples of the layer structures RCI and RCII with the variability in stacking producing high-mosaicity single crystals and a new polymorph, RCIII. One cause of this complexity, that an accessible conformational change of this molecule can substitute for the enantiomer in a low energy packing well enough to produce a solid solution (Fig. 2a), is rather unusual. However, the other, that a hydrogen bonded layer in the most stable form can stack in a variety of ways that are close in energy, is not uncommon. This study has demonstrated the consequences of the resulting difficulty in generating structurally pure samples, including variability in melting points and heats of fusion.

Acknowledgements

We thank Profs. Constantinos Pantelides and Claire Adjiman (Imperial College) for use of CrystalPredictor and CrystalOptimizer codes, David Jackson for solid-state NMR experiments, and Dr. Neil Feeder (Cambridge Crystallographic Data Centre) for assistance and valuable discussions on using the CCDC tools. This work was supported by Eli Lilly and Company through the Lilly Research Award Program (LRAP).

Appendix A. Supplementary material

CCDC 977885–977892 contains the supplementary crystallographic data for this paper. These data can be obtained free of charge via http://www.ccdc.cam.ac.uk/conts/retrieving.html (or from the Cambridge Crystallographic Data Centre, 12, Union Road, Cambridge CB2 1EZ, UK; fax: +44 1223 336033). Supplementary data associated with this article can be found, in the online version, at http://dx.doi.org/10.1016/j.molstruc.2014.01.014.

References

[1] G. Coquerel, Chem. Eng. Process. 45 (2006) 857–862.
[2] A.D. Bond, R. Boese, G.R. Desiraju, Angew. Chem., Int. Ed. 46 (2007) 618–622.
[3] G.M. Day, Crystallogr. Rev. 17 (2011) 3–52.
[4] S.L. Price, Chem. Soc. Rev. (2014), http://dx.doi.org/10.1039/C3CS60279F.
[5] S.L. Price, Acc. Chem. Res. 42 (2009) 117–126.
[6] M. Habgood, Cryst. Growth Des. 11 (2011) 3600–3608.
[7] D.A. Bardwell, C.S. Adjiman, Y.A. Arnautova, E. Bartashevich, S.X. Boerrigter, D.E. Braun, A.J. Cruz-Cabeza, G.M. Day, R.G. la Valle, G.R. Desiraju, B.P. van Eijck, J.C. Facelli, M.B. Ferraro, D. Grillo, M. Habgood, D.W. Hofmann, F. Hofmann, K.V. Jose, P.G. Karamertzanis, A.V. Kazantsev, J. Kendrick, L.N. Kuleshova, F.J. Leusen, A.V. Maleev, A.J. Misquitta, S. Mohamed, R.J. Needs, M.A. Neumann, D. Nikylov, A.M. Orendt, R. Pal, C.C. Pantelides, C.J. Pickard, L.S. Price, S.L. Price, H.A. Scheraga, J. van de Streek, T.S. Thakur, S. Tiwari, E. Venuti, I.K. Zhitkov, Acta Crystallogr., Sect. B 67 (2011) 535–551.
[8] A.V. Kazantsev, P.G. Karamertzanis, C.S. Adjiman, C.C. Pantelides, S.L. Price, P.T. Galek, G.M. Day, A.J. Cruz-Cabeza, Int. J. Pharm. 418 (2011) 168–178.
[9] S.Z. Ismail, C.L. Anderton, R.C. Copley, L.S. Price, S.L. Price, Cryst. Growth Des. 13 (2013) 2396–2406.
[10] R.M. Bhardwaj, L.S. Price, S.L. Price, S.M. Reutzel-Edens, G.J. Miller, I.D.H. Oswald, B. Johnston, A.J. Florence, Cryst. Growth Des. 13 (2013) 1602–1617.
[11] J. Kendrick, G.A. Stephenson, M.A. Neumann, F.J. Leusen, Cryst. Growth Des. 13 (2013) 581–589.
[12] J.A. Panetta, J.K. Shadle, M.L. Phillips, D.N. Benslay, P.P.K. Ho, Ann. N. Y Acad. Sci. (1993) 415–416.
[13] S.M. Reutzel-Edens, V.A. Russell, L. Yu, J. Chem. Soc. Perkin Trans. 2 (5) (2000) 913–924.
[14] J. Huang, S. Chen, I.A. Guzei, L. Yu, J. Am. Chem. Soc. 128 (2006) 11985–11992.
[15] L. Yu, J. Am. Chem. Soc. 125 (2003) 6380–6381.
[16] S.A. Chen, H.M. Xi, L. Yu, J. Am. Chem. Soc. 127 (2005) 17439–17444.
[17] C. Stoica, P. Tinnemans, H. Meekes, E. Vlieg, Cryst. Growth Des. 5 (2005) 975–981.
[18] H.H. Tung, Org. Process Res. Dev. 17 (2013) 445–454.
[19] C.C. Sun, J. Pharm. Sci. 98 (2009) 1744–1749.
[20] L. Yu, J. Huang, K.J. Jones, J. Phys. Chem. B 109 (2005) 19915–19922.
[21] T. Gelbrich, D.E. Braun, A. Ellern, U.J. Griesser, Cryst. Growth Des. 13 (2013) 1206–1217.
[22] Y.A. Abramov, J. Phys. Chem. A 115 (2011) 12809–12817.
[23] A. Otero-de-la-Roza, E.R. Johnson, J. Chem. Phys. 137 (2012) 054103.
[24] D.E. Braun, M. Ardid-Candel, E. D'Oria, P.G. Karamertzanis, J.B. Arlin, A.J. Florence, A.G. Jones, S.L. Price, Cryst. Growth Des. 11 (2011) 5659–5669.
[25] Bruker AXS Inc. SAINT. [8.32b], Madison, Wisconsin, USA, 2013.
[26] G. Sheldrick, Acta Crystallogr. Sect. A 46 (1990) 467–473.
[27] G.M. Sheldrick, SHELXTL [6.2], University of Gottingen, Germany, 2013.
[28] Bruker AXS Inc., SADABS: Area-Detector Absorption Correction [2012/1], Bruker AXS Inc., Madison, Wisconsin, USA, 2012.
[29] A.L. Spek, Acta Crystallogr. Sect. D 65 (2009) 148–155.
[30] B.M. Fung, A.K. Khitrin, K. Ermolaev, J. Magn. Reson. 142 (2000) 97–101.
[31] O.N. Antzutkin, Prog. Nucl. Magn. Reson. Spectrosc. 35 (1999) 203–266.
[32] G. Metz, X.L. Wu, S.O. Smith, J. Magn. Reson. Ser. A 110 (1994) 219–227.
[33] M.J. Frisch, G.W. Trucks, H.B. Schlegel, G.E. Scuseria, M.A. Robb, J.R. Cheeseman, J. Montgomery, T. Vreven, K.N. Kudin, J.C. Burant, J.M. Millam, S.S. Iyengar, J. Tomasi, V. Barone, B. Mennucci, M. Cossi, G. Scalmani, N. Rega, G.A. Petersson, H. Nakatsuji, M. Hada, M. Ehara, K. Toyota, R. Fukuda, J. Hasegawa, M. Ishida, T. Nakajima, Y. Honda, O. Kitao, H. Nakai, M. Klene, X. Li, J.E. Knox, H.P. Hratchian, J.B. Cross, V. Bakken, C. Adamo, J. Jaramillo, R. Gomperts, R.E. Stratmann, O. Yazyev, A.J. Austin, R. Cammi, C. Pomelli, J. Ochterski, P.Y. Ayala, K. Morokuma, G.A. Voth, P. Salvador, J.J. Dannenberg, V.G. Zakrzewski, S. Dapprich, A.D. Daniels, M.C. Strain, O. Farkas, D.K. Malick, A.D. Rabuck, K. Raghavachari, J.B. Foresman, J.V. Ortiz, Q. Cui, A.G. Baboul, S. Clifford, J. Cioslowski, B.B. Stefanov, G. Liu, A. Liashenko, P. Piskorz, I. Komaromi, R.L. Martin, D.J. Fox, T. Keith, M.A. Al Laham, C.Y. Peng, A. Nanayakkara, M. Challacombe, P.M.W. Gill, B. Johnson, W. Chen, M.W. Wong, C. Gonzalez, J.A. Pople, Gaussian 03, Gaussian Inc., Wallingford, CT, 2004.
[34] A.J. Stone, J. Chem. Theory Comput. 1 (2005) 1128–1132.
[35] A.J. Stone, A Program for Performing Distributed Multipole Analysis of Wave Functions Calculated Using the Gaussian Program System [2.2], University of Cambridge, Cambridge, United Kingdom, 2010.
[36] D.E. Williams, S.R. Cox, Acta Crystallogr., Sect. B 40 (1984) 404–417.
[37] D.S. Coombes, S.L. Price, D.J. Willock, M. Leslie, J. Phys. Chem. 100 (1996) 7352–7360.
[38] G.M. Day, T.G. Cooper, A.J. Cruz-Cabeza, K.E. Hejczyk, H.L. Ammon, S.X.M. Boerrigter, J. Tan, R.G. Della Valle, E. Venuti, J. Jose, S.R. Gadre, G.R. Desiraju, T.S. Thakur, B.P. van Eijck, J.C. Facelli, V.E. Bazterra, M.B. Ferraro, D.W.M. Hofmann, M. Neumann, F.J.J. Leusen, J. Kendrick, S.L. Price, A.J. Misquitta, P.G. Karamertzanis, G.W.A. Welch, H.A. Scheraga, Y.A. Arnautova, M.U. Schmidt, J. van de Streek, A. Wolf, B. Schweizer, Acta Crystallogr., Sect. B 65 (2009) 107–125.
[39] J.P.M. Lommerse, W.D.S. Motherwell, H.L. Ammon, J.D. Dunitz, A. Gavezzotti, D.W.M. Hofmann, F.J.J. Leusen, W.T.M. Mooij, S.L. Price, B. Schweizer, M.U. Schmidt, B.P. van Eijck, P. Verwer, D.E. Williams, Acta Crystallogr., Sect. B 56 (2000) 697–714.
[40] T.A. Halgren, J. Am. Chem. Soc. 114 (1992) 7827–7843.
[41] S.L. Price, M. Leslie, G.W.A. Welch, M. Habgood, L.S. Price, P.G. Karamertzanis, G.M. Day, Phys. Chem. Chem. Phys. 12 (2010) 8478–8490.
[42] A.V. Kazantsev, P.G. Karamertzanis, C.S. Adjiman, C.C. Pantelides, J. Chem. Theory Comput. 7 (2011) 1998–2016.
[43] T.G. Cooper, K.E. Hejczyk, W. Jones, G.M. Day, J. Chem. Theory Comput. 4 (2008) 1795–1805.
[44] C.F. Macrae, I.J. Bruno, J.A. Chisholm, P.R. Edgington, P. McCabe, E. Pidcock, L. Rodriguez-Monge, R. Taylor, J. van de Streek, P.A. Wood, J. Appl. Crystallogr. 41 (2008) 466–470.
[45] P.T.A. Galek, L. Fabian, W.D.S. Motherwell, F.H. Allen, N. Feeder, Acta Crystallogr., Sect. B 63 (2007) 768–782.
[46] P.A. Wood, T.S. Olsson, J.C. Cole, S.J. Cottrell, N. Feeder, P.T. Galek, C.R. Groom, E. Pidcock, CrystEngCommun 15 (2013) 65–72.
[47] C. Gervais, G. Coquerel, Acta Crystallogr., Sect. B 58 (2002) 662–672.
[48] A.D. Bond, CrystEngCommun 14 (2012) 2363–2366.
[49] A. Gavezzotti, J. Pharm. Sci. 96 (2007) 2232–2241.
[50] R. Herbst-Irmer, G.M. Sheldrick, Acta Crystallogr. Sect. B-Struct. Sci. 54 (1998) 443–449.
[51] T. van Mourik, P.G. Karamertzanis, S.L. Price, J. Phys. Chem. A 110 (2006) 8–12.

[52] O.G. Uzoh, A.J. Cruz-Cabeza, S.L. Price, Cryst. Growth Des. 12 (2012) 4230–4239.
[53] RCI is P21/c and the pseudo inversion centre is at approximately (0.25, 0.25, 0.25) which does not correspond to any space group. RCIII is triclinic, but with a pseudo screw axis, yet neither of the triclinic space groups have screw axes.
[54] H. Wu, M. Habgood, J.E. Parker, N. Reeves-McLaren, J.K. Cockcroft, M. Vickers, A.R. West, A.G. Jones, CrystEngCommun 15 (2013) 1853–1859.
[55] A.J. Florence, J. Bardin, B. Johnston, N. Shankland, T.A.N. Griffin, K. Shankland, Z. Kristallogr. (2009) 215–220.
[56] V.L. Deringer, V. Hoepfner, R. Dronskowski, Cryst. Growth Des. 12 (2012) 1014–1021.
[57] R.J. Davey, S.L. Schroeder, J.H. ter Horst, Angew. Chem., Int. Ed. 52 (2013) 2166–2179.
[58] J.B. Arlin, L.S. Price, S.L. Price, A.J. Florence, Chem. Commun. 47 (2011) 7074–7076.
[59] T. Friscic, L.R. MacGillivray, Chem. Commun. (2009) 773–775.
[60] D.K. Bucar, G.M. Day, I. Halasz, G.G.Z. Zhang, J.R.G. Sander, D.G. Reid, L.R. MacGillivray, M.J. Duer, W. Jones, Chem. Sci. 4 (2013) 4417–4425.
[61] A. Schoenleber, Z. Kristallogr. 226 (2011) 499–517.
[62] S.L. Price, Acta Crystallogr., Sect. B 69 (2013) 313–328.
[63] M.C. Etter, Acc. Chem. Res. 23 (1990) 120–126.
[64] A.T. Anghel, G.M. Day, S.L. Price, CrystEngCommun 4 (2002) 348–355.
[65] G.M. Day, S.L. Price, M. Leslie, J. Phys. Chem. B 107 (2003) 10919–10933.
[66] A.E. Gray, G.M. Day, M. Leslie, S.L. Price, Mol. Phys. 102 (2004) 1067–1083.
[67] M. Urbanova, A. Sturcova, J. Brus, H. Benes, E. Skorepova, B. Kratochvil, J. Cejka, I. Sedenkova, L. Kobera, O. Policianova, A. Sturc, J. Pharm. Sci. 102 (2013) 1235–1248.
[68] E. Skorepova, J. Cejka, M. Husak, V.A. Eigner, J. Rohlicek, A. Sturc, B. Kratochvil, Cryst. Growth Des. 13 (2013) 5193–5203.
[69] G. Borodi, M.M. Pop, O. Onija, X. Filip, Cryst. Growth Des. 12 (2012) 5846–5851.
[70] C. Brandel, Y. Amharar, J.M. Rollinger, U.J. Griesser, Y. Cartigny, S. Petit, G. Coquerel, Mol. Pharm. 10 (2013) 3850–3861.
[71] F.G. Vogt, R.C. Copley, R.L. Mueller, G.P. Spoors, T.N. Cacchio, R.A. Carlton, L.M. Katrincic, J.M. Kennady, S. Parsons, O.V. Chetina, Cryst. Growth Des. 10 (2010) 2713–2733.
[72] R.W. Lancaster, L.D. Harris, D. Pearson, CrystEngCommun 13 (2011) 1775–1777.
[73] R.C.B. Copley, S.A. Barnett, P.G. Karamertzanis, K.D.M. Harris, B.M. Kariuki, M.C. Xu, E.A. Nickels, R.W. Lancaster, S.L. Price, Cryst. Growth Des. 8 (2008) 3474–3481.
[74] D.E. Braun, D.A. Tocher, S.L. Price, U.J. Griesser, J. Phys. Chem. B 116 (2012) 3961–3972.
[75] M. Tremayne, L. Grice, J.C. Pyatt, C.C. Seaton, B.M. Kariuki, H.H.Y. Tsui, S.L. Price, J.C. Cherryman, J. Am. Chem. Soc. 126 (2004) 7071–7081.
[76] M.M. Hansen, A.R. Harkness, V.V. Khau, M.J. Martinelli, J.B. Deeter, Tetrahedron-Asymmetry 7 (1996) 2515–2518.
[77] E. D'Oria, P.G. Karamertzanis, S.L. Price, Cryst. Growth Des. 10 (2010) 1749–1756.